PHYSICAL REVIEW D VOLUME 51, NUMBER 1 1 JANUARY 1995

Dual parton model at cosmic ray energies

J. Ranft
Istituto Nazionale di Fisica Nucleare, Laboratori Nazionale di Frascati, I-00044 Frascati, Roma, Italy
(Received 15 July 1994)

The dual parton model for hadron-hadron, hadron-nucleus, and nucleus-nucleus collisions is studied in the fragmentation region up to the cosmic ray energy region. Because of the excellent Feynman scaling behavior of the model outside the regions around $x_F = 1$ and $x_F = 0$, it is found that accelerator data in the fragmentation region are indeed relevant for the cosmic ray energy region. However, not enough data are available in the fragmentation region of hadron collisions with light target nuclei. Therefore many features of hadron production in collisions involving nuclei can only be extracted from the study of models.

PACS number(s): 13.85.Hd, 13.85.Ni, 13.85.Tp

I. INTRODUCTION

A hadron production model to be used at cosmic ray energies should take into account all possible information from fixed target experiments and collider experiments at accelerators. There are, however, important differences: For studying the cosmic ray cascade, the main interest is in the forward fragmentation region of hadron-nucleus and nucleus-nucleus collisions. Best studied at accelerators is the central region in hadron-hadron collisions.

In this paper we will discuss hadron production in the framework of the dual parton model with emphasis on the fragmentation region. Important for cosmic ray studies are two aspects of multiparticle production: (i) the change of particle production with energy, starting from the region well studied at present accelerator experiments; (ii) the dependence of particle production on the nuclear target (and projectile).

A model for hadronic and nuclear interactions to be used in cosmic ray physics should provide the basic hadronic interaction term for the cosmic ray cascade. It should provide the cross sections for hadron-hadron, hadron-nucleus, and nucleus-nucleus collisions as function of the energy. Secondary π^0 and η mesons are the source of the electromagnetic shower; secondary $\pi^{\pm}$ and $K^{\pm}$ mesons are the source of cosmic ray muons and the source of atmospheric neutrinos produced by the cosmic ray cascade. Secondary charmed mesons are the source for prompt muons and neutrinos. The model should work from the pion production threshold up to the highest possible primary energies.

Soft multiparticle production characterizing hadronic interactions at supercollider or cosmic ray energies cannot be understood purely within theoretical approaches provided by perturbative QCD. The nonperturbative soft component of hadron production, which is responsible for all of hadron production at low energies, is still acting at higher energies.

The energy dependence of hadron production has so far been best studied in hadron-hadron collisions. With the use of basic ideas of the dual topological unitarization scheme [1,2], the dual parton model (D.P.M.) (a recent review is given in Ref. [3]) has been very successfully describing soft hadronic processes.

Observations such as rapidity plateaus and average transverse momenta rising with energy, Koba-Nielsen-Olesen (KNO) scaling violations, transverse momentum-multiplicity correlations, and *minijets* pointed out that soft and hard processes are closely related. These properties were understood within the two-component dual parton model [4–10].

The hard component is introduced applying lowest order of perturbative hard constituent scattering [11]. Single diffraction dissociation is represented by a triple-Pomeron exchange (high mass single diffraction) and a low mass component.

The dual parton model provides a framework not only for the study of hadron-hadron interactions, but also for the description of particle production in hadron-nucleus and nucleus-nucleus collisions at high energies. Within this model the high energy projectile undergoes a multiple scattering as formulated in Glaubers approach; particle production is again realized by the fragmentation of colorless parton-parton chains constructed from the quark content of the interacting hadrons.

In Sec. II we give a short account of the dual parton model. Section III describes the Monte Carlo event generator DPMJET-II used in this paper. We study with DPMJET-II hadron-hadron collisions in Sec. IV, hadron-nucleus collisions in Sec. V, and nucleus-nucleus collisions in Sec. VI. The properties of the model relevant at cosmic ray energies are discussed in Sec. VII and a summary is given in Sec. VIII.

II. THE DUAL PARTON MODEL

A. Energy dependence of multiparticle production and the two-component dual parton model for hadron-hadron collisions

The soft input cross section in our unitarization scheme is described by the supercritical Pomeron

$$\sigma_s = g^2 s^{\alpha(0)-1}, \tag{1}$$

with g being the effective proton-Pomeron coupling constant and $\alpha(0)$ the Pomeron intercept. The corresponding Pomeron trajectory is given by $\alpha(t) = \alpha(0)+\alpha' t$. The supercritical Pomeron was used in the two-component DPM from the beginning [4]. In all fits of the Pomeron parameters to cross section data, we get consistently better fits with the supercritical Pomeron than with the critical one.

In addition to the supercritical soft [Fig. 1(a)] and hard Pomerons [Fig. 1(b)] we introduce graphs with Pomeron-Pomeron couplings. Provided that the Pomeron-Pomeron coupling constant Γ is small in comparison with other couplings, such as g, it is sufficient to consider the expansion in Γ only up to first order [5]. Thus a correction to the pure Pomeron exchange is represented by the triple-Pomeron graph [Fig. 1(c)] included with an input cross section

$$\sigma_{\rm TP} = \frac{2}{16\pi}\frac{g^3\Gamma}{b_{\rm TP}} \ln\frac{s}{s_0}, \tag{2}$$

where $b_{\rm TP}$ is the slope $b_{\rm TP} = b^0_{\rm TP}+2\alpha' \ln(s)$ and $s_0 = 100$ GeV^2. In Ref. [10] we report on the fit of the model parameters to the cross section data using many different parton structure functions. In DPMJET we use the Martin-Roberts-Stirling set D$_-$ (MRS[D$_-$]) structure functions, for which we obtain the parameters $g^2 = 55.96$ mb, $\alpha(0) = 1.049$, $\alpha' = 0.351$, $b = b^0_{\rm TP} = 1.04$ GeV^{-2} and $b_h = 2.01$ GeV^{-2} [see also Eq. (6)]. The simplest cut of the triple-Pomeron [Fig. 1(c)] corresponds to a high mass single diffractive interaction. High mass diffraction is a comparatively rare process. High mass means that the diffractively excited system should not be a well-defined hadron resonance. We also describe high mass double diffractive processes again to first order introducing loop graphs [Fig. 1(d)], with a cross section

$$\sigma_L = \frac{1}{16\pi}\frac{g^2\Gamma^2}{2b_{\rm DD}}\left(\ln^2\frac{s}{s_0}+\ln^2\frac{s'_0}{s}-2\ln^2\frac{5}{20}\right), \tag{3}$$

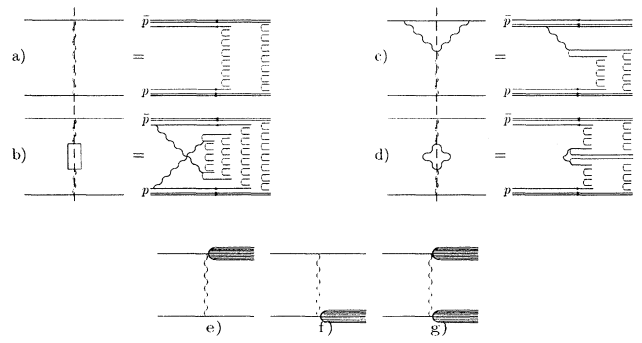

FIG. 1. Diagrams and the corresponding cut graphs for the exchange of (a) one soft Pomeron, (b) one hard Pomeron, and (c) one triple-Pomeron (high mass single diffraction). (d) shows one cut Pomeron-loop graph (high mass double diffraction). Low mass single diffractive processes (e), (f) and low mass double diffractive processes (g) are introduced via a two-channel Eikonal formalism.

with $b_{\rm DD}$ being the slope parameter $b_{\rm DD} = 2\alpha' \ln(s)$, $s_0 = 400$ GeV^2, and $s'_0 = 25$ GeV^2.

The input cross section for semihard multiparticle production σ_h is calculated applying the QCD improved parton model; the details are given in Refs. [4,7,8,12]:

$$\sigma_h = \sum_{i,j}\int_0^1 dx_1 \int_0^1 dx_2 \times \int d\hat{t}\frac{1}{1+\delta_{ij}}\frac{d\sigma_{{\rm QCD},ij}}{d\hat{t}} f_i(x_1,Q^2) f_j(x_2,Q^2) \times\Theta(p_\perp - p_{\perp_{\rm thr}}). \tag{4}$$

$f_i(x,Q^2)$ are the structure functions of partons with the flavor i and scale Q^2, and the sum i,j runs over all possible flavors. To remain in the region where perturbation theory is valid, we use a low $p_\perp$ cutoff $p_{\perp_{\rm thr}}$ for the minijet component. Furthermore, since we calculate $\sigma_{{\rm QCD},ij}$ in lowest order QCD perturbation theory we multiply the hard input cross section σ_h with a K factor in the range of 1.5–2. A hard interaction leads to a chain system shown in Fig. 1(b).

The momentum fractions of the constituents at the ends of the different chains are sampled using the exclusive parton distribution, which has the form for an event with n_s soft and $n_h (n_h \geq 1)$ hard Pomerons:

$$\rho(x_1,\ldots,x_{2n_s},\ldots,x_{2n_s+2+n_h}) \sim \frac{1}{\sqrt{x_1}}\left(\prod_{i=3}^{2n_s+2}\frac{1}{\sqrt{x_i}}\right)x_2^{1.5} \times \prod_{i=2n_s+3}^{2n_s+2+n_h} g(x_i,Q_i)\,\delta\left(1-\sum_{i=1}^{2n_s+2+n_h} x_i\right). \tag{5}$$

The distributions $g(x_i,Q_i)$ are the distribution functions of the partons engaged in the hard scattering. The Regge behavior of the soft valence quark x distributions is $x^{-0.5}$; the term $1/\sqrt{x_1}$ refers to the valence quark at the end of a soft valence chain. The Regge behavior of a diquark x distribution is $x^{1.5}$; the term $x_2^{1.5}$ refers to the x distribution of the valence diquark at the end of a soft valence chain. The Regge behavior of soft sea-quark x distributions agrees with the one of the valence quarks; it is also $x^{-0.5}$. The terms $1/\sqrt{x_i}$ refer to the sea quarks and sea antiquarks at the end of soft sea chains.

Here one remark is in order. In the previous papers [5,10] we did use the terms $1/x_i$ for the soft sea quarks and antiquarks. A corresponding formula with $1/x_i$ is also given in the dual parton model review [3]. The use of this different behavior for the soft sea-quark x distributions was certainly motivated by the behavior of the deep inelastic x distributions for sea quarks, but it is not correct for the soft sea quarks. The correct Regge behavior of soft sea quarks was already discussed in an appendix to the paper of Capella and Tran Thanh Van [13] and it is also given for instance, in [14]. It is easy to check that at low energies, typical for fixed target experiments, the correct form $1/x$ or $1/\sqrt{x}$ is not very important; the behavior is mainly determined by the low x cutoff of the

structure functions. But for our goal, to study the Feynman x_F distributions of hadrons at the highest energies in the fragmentation region; it is essential to use the correct form $1/\sqrt{x}$.

Soft (s), hard (h), high mass single diffractive (TP), and high mass double diffractive(L) processes are treated simultaneously within an Eikonal unitarization scheme using the impact parameter representation

$$\chi_i(B,s) = \frac{\sigma_i(s)}{8\pi b_i} \exp\left(-\frac{B^2}{4b_i}\right), \quad i = s,h,\mathrm{TP},L \qquad (6)$$

normalized by

$$\int 2\chi_i(B,s)d^2B = \sigma_i \qquad (7)$$

with b_h energy independent, $b_s = b_{\mathrm{TP}} = b_L = b+\alpha' \ln(s)$. The exclusive cross section for l_c cut soft Pomerons, m_c cut hard Pomerons, n_c cut triple-Pomeron graphs, and p_c cut loop graphs is given by

$$\sigma(l_c,m_c,n_c,p_c,B,s) = \frac{(2\chi_s)^{l_c}}{l_c!}\frac{(2\chi_h)^{m_c}}{m_c!}\frac{(-2\chi_{\mathrm{TP}})^{n_c}}{n_c!} \times \frac{(-2\chi_L)^{p_c}}{p_c!}\exp[-2\chi(B,s)] \qquad (8)$$

with

$$\chi(B,s) = \chi_s(B,s) + \chi_h(B,s) - \chi_{\mathrm{TP}}(B,s) - \chi_L(B,s). \qquad (9)$$

The total and elastic cross sections are given by

$$\sigma_{\mathrm{tot}} = 4\pi \int_0^\infty B\,dB(1-\exp[\chi(B,s)]),$$
$$\sigma_{\mathrm{el}}(B,s) = \tfrac{1}{4}[\sigma_{\mathrm{tot}}(B,s)]^2. \qquad (10)$$

Diffractive processes characterized by the excitation of an initial hadron to intermediate resonances (low mass diffractive interactions) are introduced via a two-channel Eikonal formalism. As suggested in Ref. [5], a new coupling λ modifies the three graphs given in Figs. 1(e)–1(g) and leads to a modification of each graph with l soft, m hard, n triple-Pomeron, and p loop exchanges.

During 1992–1993 new data on deep inelastic scattering and new fits to parton structure functions were reported. New features of these fits include (i) the flavor dependence of sea-quark distributions and (ii) a stronger rise of the structure functions at low x values, that is, in the region important for minijets. These fits by Martin, Roberts, and Stirling [15] and by the CTEQ Collaboration [16] include functions with a conventional $1/x$ singularity of sea-quark and gluon distributions (for instance, the MRS [D_0] functions) as well as functions with a $1/x^{1.5}$ singularity (for instance, the MRS [D_-] functions). The measurements previous to the DESY ep collider HERA did not allow us to decide between these two possibilities. However, there were theoretical arguments in favor of the $1/x^{1.5}$ singularity [17]. These more singular parton distributions were in the past used to calculate the minijets [7,8], but not taken very seriously. This was changed in [10], since the first HERA data seem to favor just these singular parton distribution functions [18].

Gluons are the most important source of minijets; unfortunately, so far no HERA data for the gluon distributions are available, but we should start now to discuss the implementation of the more singular functions for minijets.

In order to remove an inconsistency in older versions of DTUJET with $x^{-1.5}$ singular structure functions we make in DTUJET-93 [10] the threshold for minijet production $p_{\perp_{\mathrm{thr}}}$ energy dependent in such a way that at no energy and for no parton distribution function (PDF) is the resulting σ_h bigger than the total cross section. Then at least we have a cross section, which is indeed mainly the cross section of a $2 \to 2$ parton process at this level, but we can get back to the real $2 \to n$ processes via parton showering. One possible form for this energy-dependent cutoff is

$$p_{\perp_{\mathrm{thr}}} = 2.5 + 0.12[\log_{10}(\sqrt{s}/\sqrt{s_0})]^3 \ [\mathrm{GeV}/c],$$
$$\sqrt{s_0} = 50 \ \mathrm{GeV}. \qquad (11)$$

The resulting σ_h are smaller than the total cross sections resulting after the unitarization for all MRS-92 and CTEQ PDF's and also the older Kwiecinski-Martin-Roberts-Stirling (KMRS) [19] distributions.

DTUJET-93 [10] has been compared with nearly all aspects of hadron production in the central region as found at the CERN and Fermilab colliders. Extrapolating to CERN Large Hadron Collider (LHC) energies, we get charged plateaus of 5–6 particles per pseudorapidity unit for the models with all MRS-92 and CTEQ PDF's. However, the average transverse momenta in the models with the singular PDF's rise more steeply with energy than in previously published versions of DTUJET. We find using DTUJET-93 at LHC energies an average $p_\perp$ typically 100 MeV/c bigger than previously.

The two-component dual parton model has some natural way to cut off the singularity of the minijet cross section at low $p_\perp$. The model uses the soft Pomeron cross section as the low $p_\perp$ limit of the minijets.

B. The dual parton model for hadron production in hardon-nucleus and nucleus-nucleus collisions

The first successful applications of the Monte Carlo version of the dual parton model (DPM) to hadron-nucleus [20,21] and nucleus-nucleus [22–24] collisions also demonstrated that the cascade of created secondaries in the target (and projectile) nuclei contributes significantlyj to particle production in the target (and projectile) fragmentation regions. On the other hand, it has been known for many years that a naive treatment of intranuclear cascade processes on the basis of elementary cross sections overestimates the particle yields, if the incident energy significantly exceeds 5 or 10 GeV [25,26].

This problem may be solved by introducing the concept of a formation zone [27,28], suppressing in a natu-

ral way the cascading of high-energy secondaries. The Monte Carlo model includes intranuclear cascade processes of the created secondaries combined with the formation time concept since the version DTUNUC-1.00.

In the following we briefly sketch the basic ideas of the model and mention the most important ingredients; for a more detailed description of the model as applied in the code we refer readers to Refs. [20,21,29–31,33].

1. *The Monte Carlo realization of the dual parton model DTUNUC for hadron-nucleus and nucleus-nucleus collisions*

The model starts from the impulse approximation for the interacting nuclei—i.e., with a frozen discrete spatial distribution of nucleons sampled from standard density distributions [34]. The primary interaction of the incident high-energy projectile proceeds via totally n elementary collisions between $n_p = n_A$ and $n_t = n_B$ nucleons from the projectile (for incident hadrons $n_p = 1$) and the target nuclei, respectively. Actual numbers n, n_p, and n_t are sampled on the basis of Glauber's multiple scattering formalism using the Monte Carlo algorithm of Ref. [34]. Note that individual hadrons may undergo several interactions. Particle production in each elementary collision is described in DTUNUC by the fragmentation of two color-neutral parton-parton chains. In DPMJET also multiple soft chains and multiple minijets are considered. Those chains are constructed from the valence quark systems or, in the case of repeated scatterings of single hadrons, from sea-$q\bar{q}$ pairs and sea-qq-$\bar{q}\bar{q}$ pairs of the interacting hadrons.

For nucleus-nucleus collisions in the two-chain approximation, the single-particle densities are given by

$$\begin{aligned} dN^{AB} = \frac{1}{\sigma_{AB}} \sum \sigma_{n_A,n_B,n} (\Theta(n_B - n_A)\{n_A(N^{qq^A - q_v^B} + N^{q_v^A - qq^B}) \\ +(n_B - n_A)[(1-\alpha)(N^{q_s^A - qq^B} + N^{\bar{q}_s^A - q_v^B}) + \alpha(N^{(\bar{q}\bar{q})_s^A - qq^B} + N^{(qq)_s^A - q_v^B})] \\ +(n - n_B)[(1-2\alpha)(N^{q_s^A - \bar{q}_s^B} + N^{\bar{q}_s^A - q_s^B}) \\ +\alpha(N^{q_s^A - (qq)_s^B} + N^{(qq)_s^A - q_s^B}) + \alpha(N^{\bar{q}_s^A - (\bar{q}\bar{q})_s^B} + N^{(\bar{q}\bar{q})_s^A - \bar{q}_s^B})]\} \\ +(A \to B)) \end{aligned} \tag{12}$$

Here n denotes the total number of inelastic collisions between n_A and n_B participating nucleons from the projectile and target nuclei, and α is the rate of diquark pairs to q-$\bar{q}$ pairs in the proton sea.

The hadronization of single chains is handled by the Monte Carlo codes BAMJET [35,36] and DECAY [37] or by the Lund code JETSET-7.3 [38].

2. *The Cronin effect*

In nuclear collisions, the partons at the sea and valence chain ends carry transverse momenta from different sources: (i) the intrinsic parton transverse momentum in the hadron; (ii) a transverse (and longitudinal) momentum resulting from the Fermi motion of the nucleons inside the nucleon. These first two kinds of transverse momentum were implemented into DTUNUC from the beginning; (iii) during the passage of the chain and partons through nuclear matter, they suffer nuclear multiple scattering which changes (usually increases) their transverse momenta.

The multiple scattering of partons is known since a long time to be responsible for the so-called *Cronin effect* [39] of particle production at large transverse momentum on nuclear targets. A similar enhancement of particle production in hadron-nucleus and nucleus-nucleus collisions compared to hadron-hadron collisions has been observed in many experiments already at rather modest $p_\perp$. (See, for instance, the review of experimental data of Schmidt and Schukraft [40], where the data of these $p_\perp$ ratios are collected in Figs. 4.21 to 4.24 of that reference.)

At large $p_\perp$ this effect can be studied calculating the parton scattering pertubatively. Our rather low $p_\perp$ sea chain ends might be considered as the low $p_\perp$ limit of perturbatively scattered partons. We apply to them and to the hard scattered partons multiple scattering, taking into account their path length inside the nuclear matter and adjust the parameters in such a way that the measured $p_\perp$ ratios at rising transverse momenta are approximately reproduced by the code DTUNUC.

3. *Production of strange particles*

Studies of strangeness production within this model were given in [32,33]. The DPM is an independent string model. Since the individual strings are universal building blocks of the model, the ratio of *produced* strange particles to nonstrange ones will be approximately the same in all reactions. However, since some strings contain sea quarks at one or both ends and since strange quarks are present in the proton sea, it is clear that, by increasing the number of those strings, the ratio of strange to nonstrange particles will increase. This will be the case for instance, when increasing the centrality in a nucleus-nucleus collision. It is obvious that the numerical impor-

tance of the effect will depend on the assumed fraction of strange over nonstrange quarks in the proton sea. The rather extreme case leading to a maximum increase of strangeness is to assume a SU(3) symmetric sea (equal numbers of u, d, and s flavors). We express the amount of SU(3) symmmetry of the sea chain ends by our parameter $s^{\rm sea}$ defined as $s^{\rm sea} = 2\langle s_s\rangle/(\langle u_s\rangle + \langle d_s\rangle)$, where the $\langle q_s\rangle$ give the average numbers of sea quarks at the sea chain ends. All results from DPMJET-II given in this paper are obtained with $s^{\rm sea} = 0.5$. However, the above scenario has an important drawback. Since an antiquark from the sea is always attached to a valence or sea quark on the opposite hemisphere, and since the only important strings at CERN energies are those containing at least a diquark at one end, it will be impossible to obtain an enhancement of antibaryons. In fact, because of energy-momentum conservation, the ratio $\bar{\Lambda}/h^-$ will in fact decrease with increasing centrality. In an attempt to solve this problem, we allow the creation of qq-$\bar{q}\bar{q}$ pairs from the proton sea, leading to the production of strings of type $\bar{q}\bar{q}$-$\bar{q}$ or $\bar{q}\bar{q}$-qq in which the production of strange antibaryons will be easier. The rate α of diquark pairs to q-$\bar{q}$ pairs in the proton sea is assumed to be the same as the ratio of $q \to (qq)$ to $q \to q$ branching in the chain fragmentation.

4. *Diffractive events*

Single diffraction within the dual parton model was studied in detail and compared to experimental data in [9,41]. Single diffraction dissociation is represented by a triple-Pomeron exchange (high mass single diffraction) and a low mass component (low mass single diffraction) [5].

Diffractive processes characterized by the excitation of an initial hadron to intermediate resonances (low mass diffractive interactions) are introduced via a two-channel Eikonal formalism.

III. THE EVENT GENERATOR DPMJET-II

The event generator DPMJET-I for hadron-hadron, hadron-nucleus, and nucleus-nucleus collisions described in [42] was based on DTUNUC-1.0 [43] and DTUJET-90 [5]. DPMJET-I uses the dual parton model for nuclear collisions as implemented in DTUNUC-1.0, but for each elementary nucleon-nucleon collision the full system of multiple soft chains and multiple minijets as implemented in DTUJET-90 is used. DPMJET-I was mainly used in the past to study nucleus-nucleus collisions at the energies of the CERN Super Proton Synchrotron (SPS) and the future heavy ion colliders such as the BNL Relativisitic Heavy-Ion Collider (RHIC) and CERN-LHC [42].

DPMJET, version II, is a code similar to DPMJET-I, but it has been constructed completely new on the basis of the much improved codes DTUNUC-1.04 [33] and DTUJET-93 [10]. Here we report on the study, using DPMJET-II of hadron-hadron, hadron-nucleus, and nucleus-nucleus collisions in the cosmic ray energy region. No similar studies were undertaken with the previous version of DPMJET. So far no central nucleus-nucleus collisions at RHIC or the CERN-LHC were simulated with DPMJET-II; this will be done in due course. We expect with DPMJET-II mainly a rise of the average transverse momenta in nucleus-nucleus collisions against DPMJET-I. The reason for this is the increase of average transverse momenta at c.m. system (c.m.s.) energies in the TeV region in DTUJET-93 against DTUJET-90 and the implementation of the Cronin effect in DTUNUC-1.04 (and with this in DPMJET-II). This leads to a further rise of average transverse momenta in hadron-nucleus and nucleus-nucleus collisions against hadron-hadron collisions.

IV. HADRON-HADRON COLLISIONS WITH DPMJET-II

A. Proton-proton collisions

1. *Average multiplicities of produced hadrons in p-p collisions*

DPMJET-II, using the multiple soft chains and multiple minijets from DTUJET-93, is expected to show the same rise as DTUJET-93 with energy of average multiplicities, the rapidity plateau and of average transverse momenta.

In Table I we compare DPMJET-II at 200 GeV with multiplicities of the most important secondary hadrons. The data are from Ref. [44]. The agreement is excellent.

2. *Feynman scaling*

The relevance of an event generator such as DPMJET-II based on the dual parton model for hadron production cross sections in the cosmic ray energy region can only be claimed if the model (i) agrees to the best available data in the accelerator energy range and (ii) shows a smooth behavior in the extrapolation to higher energies.

For the cosmic ray cascade in the atmosphere, only hadron-nucleus collisions are relevant, with nitrogen N

TABLE I. Comparison of average multiplicities of produced hadrons in proton-proton collisions at 200 GeV. The experimental data are from Ref. [44].

Particle	DPMJET-II	Expt.
$n_{\rm ch}$	7.66	7.69±0.06
n_-	2.82	2.85±0.03
p	1.34	1.34±0.15
n	0.62	0.61±0.30
π^+	3.17	3.22±0.12
π^-	2.56	2.62±0.06
π^0	3.38	3.34±0.24
K^+	0.28	0.28±0.06
K^-	0.19	0.18±0.05
K^0_S	0.22	0.17±0.01
$\bar{p}$	0.07	0.05±0.02

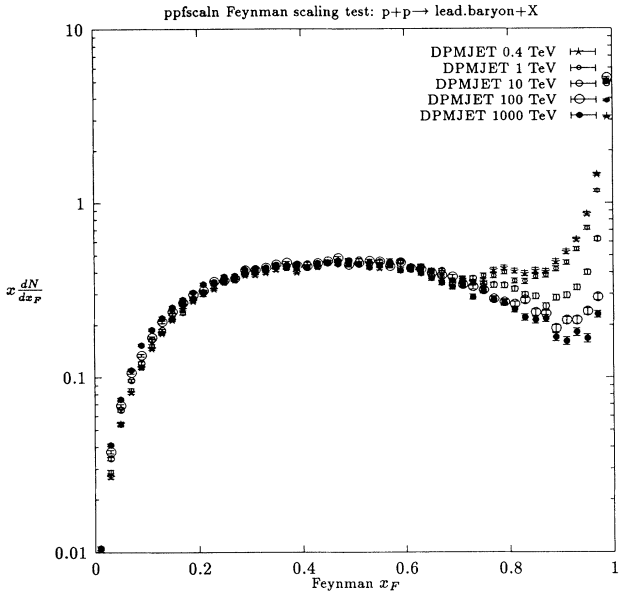

FIG. 2. Test of Feynman scaling in the production of leading baryons in proton-proton collisions. The Feynman-x distributions were calculated with the dual parton model DPMJET-II.

being the most important target nucleus. However, experimental data in the projectile fragmentation region are of much better quality in hadron-hadron, and especially proton-proton, collisions than in collisions of hadrons with light nuclei. Therefore, we start with the study of proton-proton collisions.

In order to see whether data in the accelerator energy range with projectile energies well below 1 TeV are

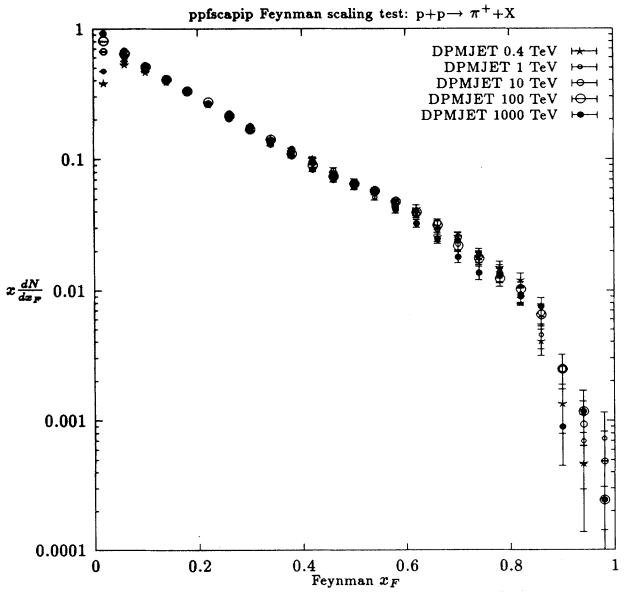

FIG. 3. Test of Feynman scaling in the production of π^+ in proton-proton collisions. The Feynman-x distributions were calculated with the dual parton model DPMJET-II.

relevant at all, we study first the Feynman scaling behavior of the model. In Figs. 2 and 3 we study the Feynman scaling of the produced leading baryons and the secondary π^+ mesons. In most of the x_F region, say for $0.05 \leq x_F \leq 0.8$, we find Feynman scaling indeed very well satisfied in the dual parton model. The violations of Feynman scaling, which occur around $x_F = 0$, are connected with the well-known rise of the rapidity plateau for all kinds of produced particles. This violation is only absent for the leading baryon, where the x_F distribution vanishes at $x_F = 0$. We find also a strong violation of Feynman scaling for secondary nucleons around $x_F = 1$. This is connected with the diffractive component, which clearly violates Feynman scaling. For produced mesons, the statistics are not good enough to conclude whether Feynman scaling near $x_F = 1$ is strongly violated, but the diffractive component should also lead to a violation for the meson distributions. However, in the Feynman x_F region most important for the cosmic ray cascade $0.1 \leq x_F \leq 0.6$, Feynman scaling also for the meson distributions is excellent. This means, within the framework of the dual parton model, experimental data in the fragmentation region (and the agreement of the model to them) are indeed very relevant also for the cosmic ray energy region.

3. Comparing to experimental Feynman x_F distributions

In proton-proton collisions, we have the advantage that experimental data are available for Feynman x_F distributions $d\sigma/dx_F$ or $x_F d\sigma/dx_F$ integrated over transverse momentum. In hadron-nucleus collisions nearly all data are only double differential distributions. In the Monte Carlo calculation, we get much smaller error bars for single differential distributions than for double differential distributions. However, also in proton-proton collisions, the data at times contradict each other.

Let us start to discuss π^+ and π^- production. The EHS-NA22 Collaboration [45] has data on $d\sigma/dx_F$ in 250 GeV proton-proton collisions. In Fig. 4 we compare the DPMJET results for π^- production in the forward and backward fragmentation regions and find a reasonable agreement. In Fig. 5 we compare the DPMJET results with the production of positively charged hadrons for $x_F \geq -0.4$ and with π^+ production for $x_F \leq -0.4$; again the agreement is reasonable. In the projectile fragmentation region at large x_F this distribution is dominated by the leading protons from diffractive and nondiffractive events.

Comparing with π^+ and π^- production from other experiments, we get problems. In Fig. 6 we compare with data from Aguilar-Benitez *et al.* [46] and Bailly *et al.* [47] for $x_{F,\mathrm{lab}} d\sigma/dx_{F,\mathrm{lab}}$ at 400 and 360 GeV. Because of the excellent Feynman scaling found above, we have these two comparisons in one plot. In the case of π^- production in Fig. 6 both sets of data agree very well and the model also agrees very well with the data in the region $x_{F,\mathrm{lab}} \leq 0.5$, where the error bars are small. Contrarily, in the case of π^+ production (not shown) both

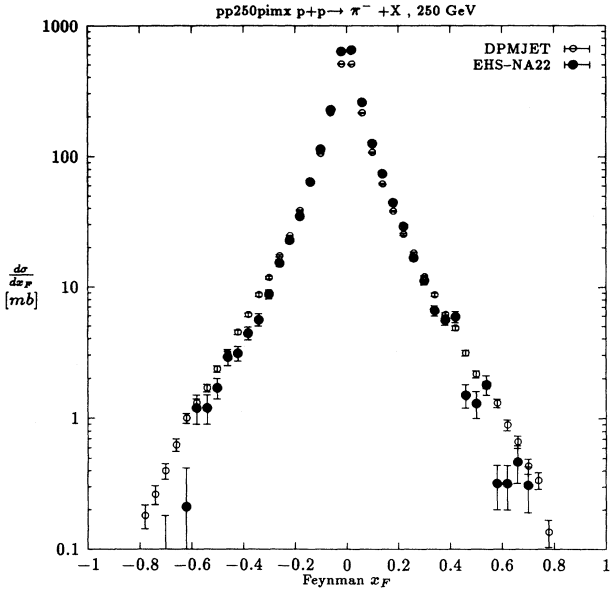

FIG. 4. Comparison of Feynman-x distributions of π^- mesons produced in proton-proton collisions at 250 GeV. The experimental data are from the EHS-NA22 Collaboration [45]. The calculation uses the dual parton model DPMJET-II.

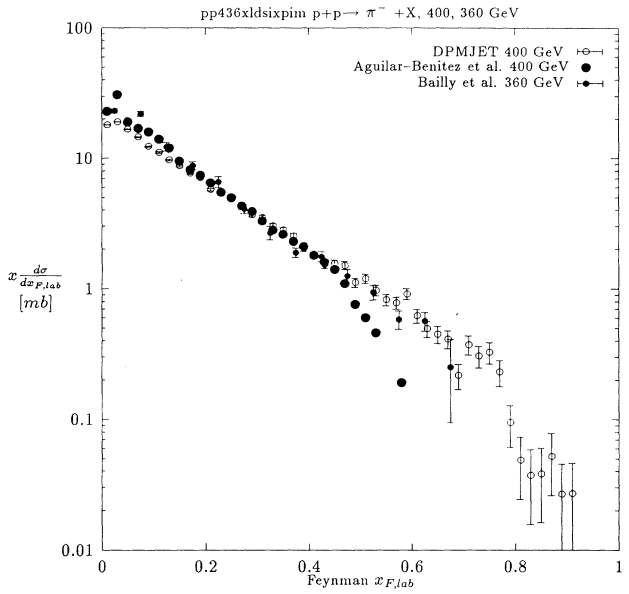

FIG. 6. Comparison of Feynman-x distributions of π^- mesons produced in proton-proton collisions at 400 and 360 GeV. The experimental data are from the Aguilar-Benitez *et al.* [46] and EHS-RCBC-Collaborations [47]. The data from both experiments agree rather well with each other, in fact most of the data points of [47] are below the [46] data. The calculation uses the dual parton model DPMJET-II.

sets of data disagree strongly (this was already noted by Aguilar-Benitez *et al.* [46]). Furthermore, the data of Aguilar-Benitez *et al.* show a strange structure at $0.5 \leq x_{F,\mathrm{lab}} \leq 0.8$, which is not found in other experiments and in the model. Finally, we note that the model is well below the data of Bailly *et al.* [47]. It seems that

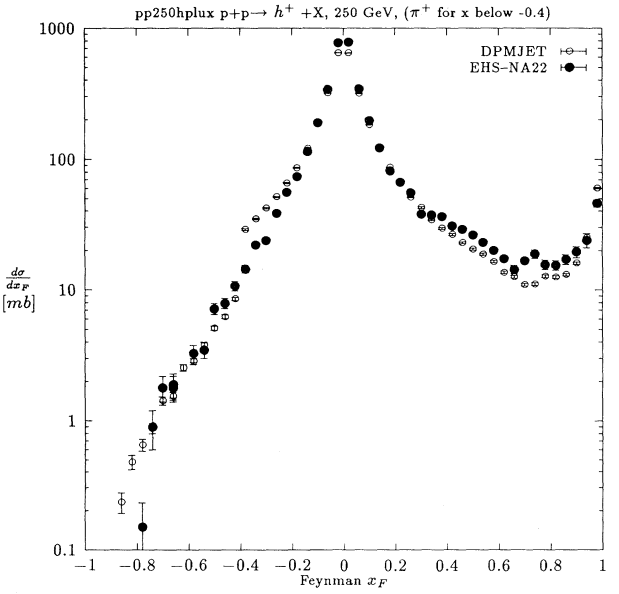

FIG. 5. Comparison of Feynman-x distributions of positively charged hadrons produced in proton-proton collisions at 250 GeV. The experimental data are from the EHS-NA22 Collaboration [45]. For $x_F \leq -0.4$ the experimental and calculated distributions refer to π^+ only. The calculation uses the dual parton model DPMJET-II.

there is an error in the normalization of these data; therefore, we ignore the comparison with these data.

We turn to the comparison with the data of Kafka *et al.* [48] and Brenner *et al.* [49] at 205 and 175 GeV. Because of the excellent Feynman scaling found above, we again compare to both experiments in one plot, Fig. 7 for π^+. This time we find for π^+ a very good agreement of both experiments, but the two sets of π^- data (not shown) are not fully consistent. In the low $x_{F,\mathrm{lab}}$ region with good statistics, we find the model for π^+ production is slightly below the data; in addition, at large $x_{F,\mathrm{lab}}$, in the region dominated by diffractive production, there is evidence that the model overestimates the π^+ as well as π^- production. This region is, however, not the dominant region, from where cosmic ray muons result.

There seems to be an inconsistency between the multiplicities compared in Table I with data and the comparison of the x_F distributions near to $x_F = 0$ with data in Figs. 4–7. In Table I we find a very good agreement between the average multiplicities, but in Figs. 4–7 at $x_F = 0$ the model is below the data. The reasons for this different normalization is not clear. The model calculation includes in all cases diffractive events; this leads certainly to smaller central multiplicities than in nondiffractive events. However, in Fig. 5 we see the diffractive component also in the data. A different binning could give a different normalization at $x_F = 0$, but in Figs. 4 and 5 the binnings of the experimental data and for the model are identical. In Figs. 6 and 7 the agreement with the data was improved near $x = 0$ by using $x_{F,\mathrm{lab}}$ for

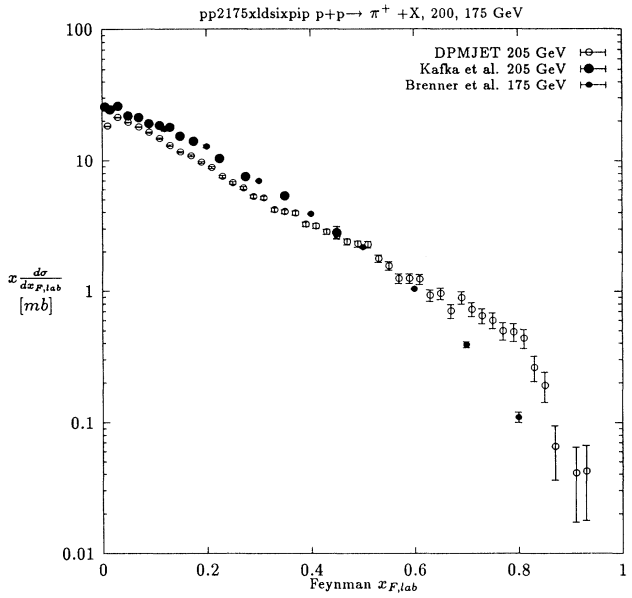

FIG. 7. Comparison of Feynman-x distributions of π^+ mesons produced in proton-proton collisions at 205 and 175 GeV. The experimental data are from Kafka *et al.* [48] and from Brenner *et al.* [49]. The data from both experiments agree rather well with each other. The calculation uses the dual parton model DPMJET-II.

the model, but again a small discrepancy remains near $x = 0$.

4. *Transverse momentum dependence of DPMJET-II in proton-proton collisions and the seagull effect*

In Fig. 8 we repeat one of the comparisons already performed with DTUJET-93 [10], this time with DPMJET-

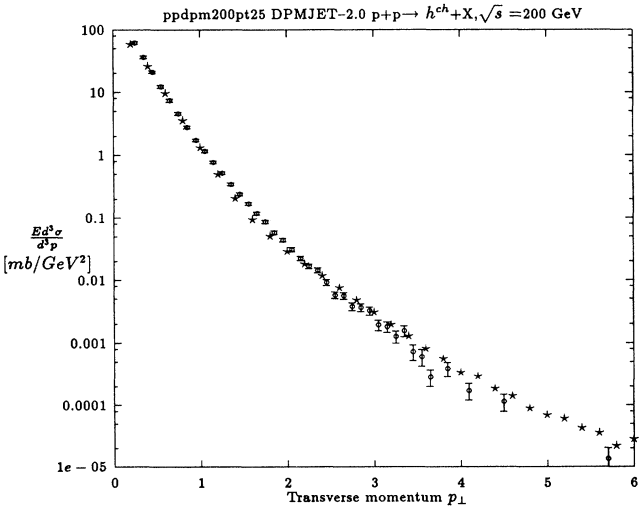

FIG. 8. Comparison of transverse momentum distributions with collider data at $\sqrt{s} = 200$ GeV [72]. The calculation uses the dual parton model DPMJET-II.

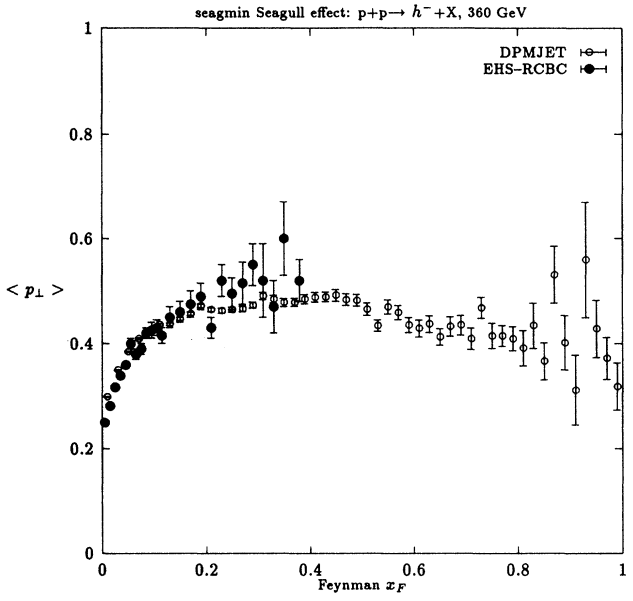

FIG. 9. Comparison of the seagull effect in the reaction $p+p \to h^- + X$ at 360 GeV. the data are from the EHS-RCBC Collaboration [73]. The calculation uses the dual parton model DPMJET-II.

II, and find the same agreement with the collider data on the $p_\perp$ distribution at $\sqrt{s} = 200$ GeV. The comparison in Fig. 8 is for the central region with pseudorapidities $|\eta| \leq 2.5$. This is not very relevant for the fragmentation region. In the fragmentation region the transverse momentum distributions and average transverse momenta are known to depend strongly on Feynman x_F. This ef-

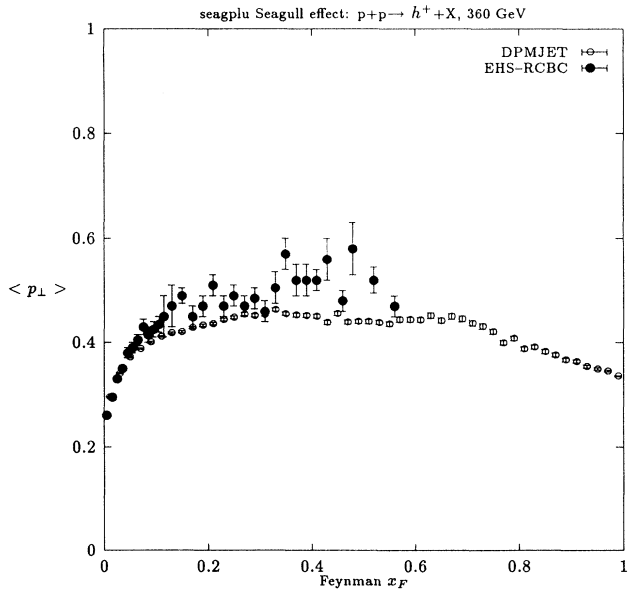

FIG. 10. Comparison of the seagull effect in the reaction $p+p \to h^+ + X$ at 360 GeV. The data are from the EHS-RCBC Collaboration [73]. The calculation uses the dual parton model DPMJET-II.

fect is known under the name *seagull effect.* In Figs. 9 and 10 we compare DPMJET-II with data on the seagull effect measured by the EHS-RCBC Collaboration at 360 GeV and find a reasonable agreement. Unfortunately, experimental data on the seagull effect are usually limited to $x_F \leq 0.5$–0.6.

5. *Strange particle production in the fragmentation region of proton-proton collisions*

Charged K mesons are, aside from the charged pions, the most important source of cosmic ray muons and neutrinos. Therefore, we have to check how well the strange hadron production is described by DPMJET-II. In Fig. 11 we compare the K^+ distribution $x_F d\sigma/dx_F$ with data from Aguilar-Benitez *et al.* [46] at 400 GeV. The agreement is reasonable, but the model does not reproduce the structure seen in the data.

In Fig. 12 we compare $x_F d\sigma/dx_F$ for Λ hyperons with the experiments of Kichimi *et al.* [50] at 400 GeV and of Bailly *et al.* [51] at 360 GeV. The agreement of both experiments with each other and the agreement of model and data are excellent, but the experimental errors and the statistical errors of the Monte Carlo calculation are quite big. In Fig. 13 we compare the K^0_S distributions from the same two experiments. At small values of x_F, where the statistics of data and Monte Carlo calculation is still good enough, we find good agreement.

In Fig. 14 we compare with the data for the seagull effect for Λ production; the agreement is reasonable. The model reproduces for Λ production the remarkable feature of the data that the average transverse momentum is nearly independent on x_F.

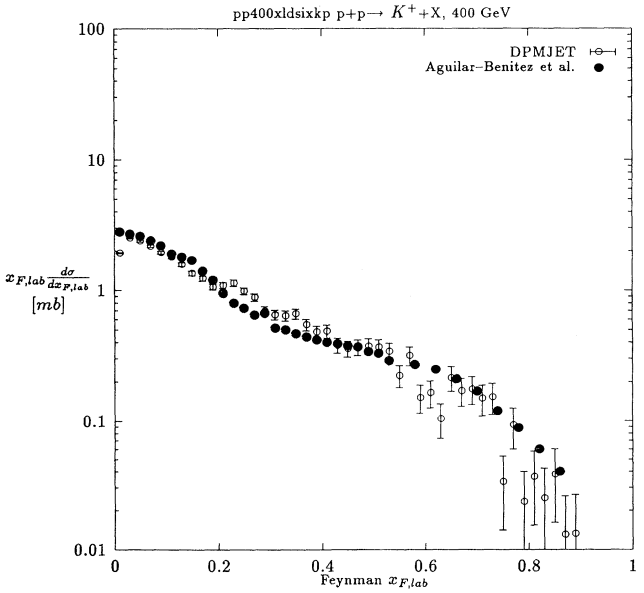

FIG. 11. Comparison of Feynman-x distributions of K^+ mesons produced in proton-proton collisions at 400 GeV. The experimental data are from the LEBC-EHS Collaboration [46]. The calculation uses the dual parton model DPMJET-II.

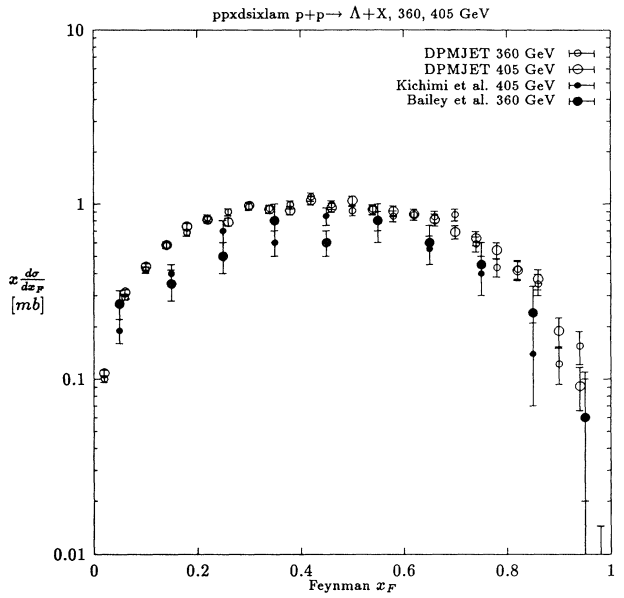

FIG. 12. Comparison of Feynman-x distributions of Λ-hyperons produced in proton-proton collisions at 360 and 405 GeV. The experimental data are from the EHS-RCBC Collaboration [51] and from Kichimi *et al.* [50]. The calculation uses the dual parton model DPMJET-II.

Finally, in Fig. 15 we compare the K^+/π^+ ratios as a function of the transverse momentum with data of Antreasyan *et al.* [52]. The model reproduces well the rise of these ratios with transverse momentum.

A stringent test of the model and particularly of the assumption of an enhanced strange sea is provided by

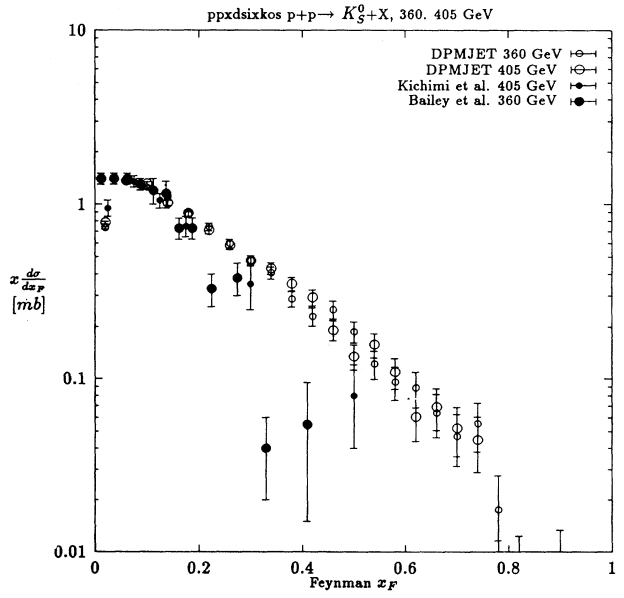

FIG. 13. Comparison of Feynman-x distributions of K^0_S mesons produced in proton-proton collisions at 360 and 405 GeV. The experimental data are from the EHS-RCBC Collaboration [51] and from Kichimi *et al.* [50]. The calculation uses the dual parton model DPMJET-II.

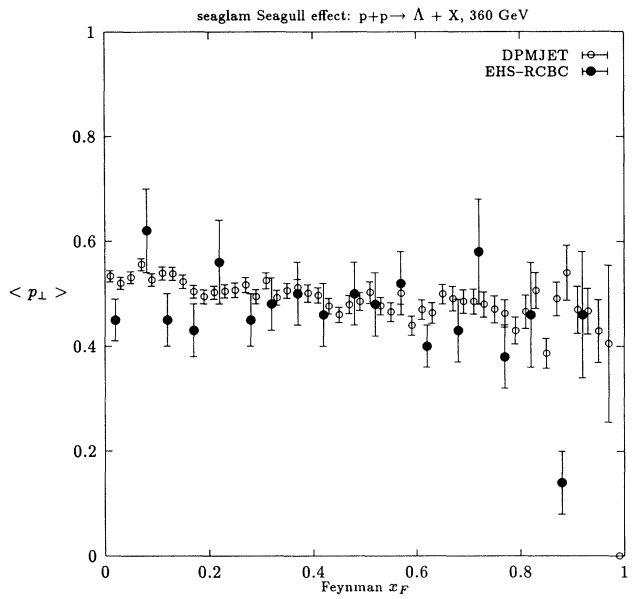

FIG. 14. Comparison of the seagull effect in the reaction $p+p \to \Lambda+X$ at 360 GeV. The data are from the EHS-RCBC Collaboration [73]. The calculation uses the dual parton model DPMJET-II.

the behavior of the average strange particle multiplicities (or, better, by the ratio of strange to nonstrange ones) as a function of either the collision energy $\sqrt{s}$ or the charged particle density. The $\sqrt{s}$ dependence is presented in Fig. 16 and the dependence on the charged plateau of the ratio K/π is presented in Fig. 17. We compare to data of the Fermilab-E735 Collaboration [53,54]. For these calculations at high energies in $p+p$ collisions we

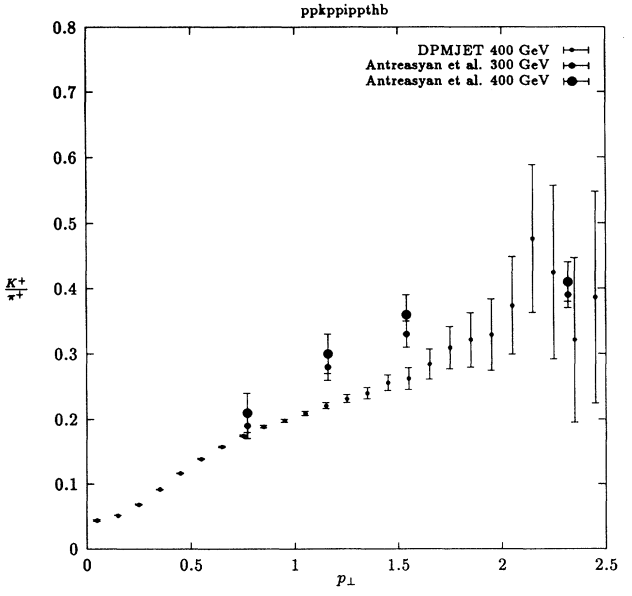

FIG. 15. The ratio K^+/π^+ as function of the transverse momentum. We compare the results of DPMJET-II at different energies to data of Antreasyan *et al.* [52].

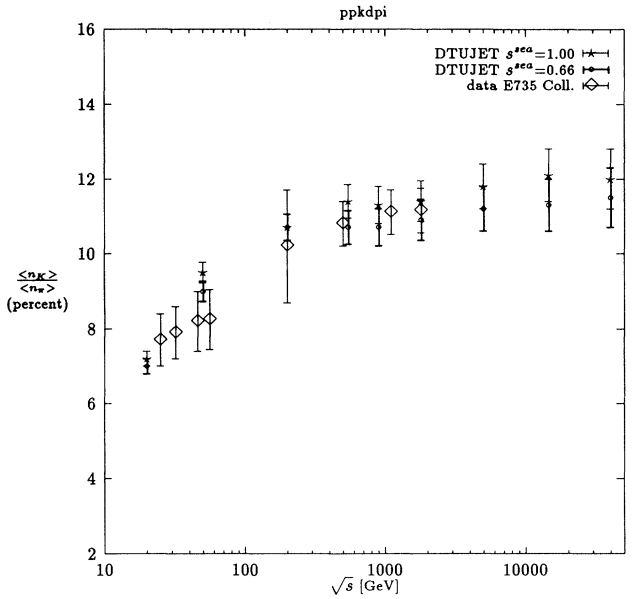

FIG. 16. K/π ratios as function of the energy $\sqrt{s}$. Calculated with the dual parton model Monte Carlo code DTUJET-93 [10] with two different values of the parameter $s^{\rm sea}$ characterizing the strange quark probability at the ends of the soft sea-sea chains and semihard chains. The experimental data are collected from the E735 Collaboration at Fermilab [53].

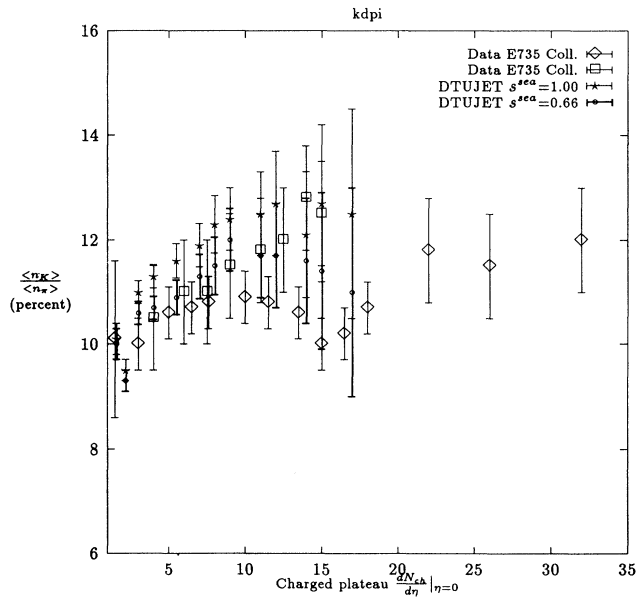

FIG. 17. K/π ratios as function of the charged plateau. Calculated with the dual parton model Monte Carlo code DTUJET-93 [10] with two different values of the parameter $s^{\rm sea}$ characterizing the strange quark probability at the ends of the soft sea-sea chains and semihard chains. The experimental data are from the E735 Collaboration at Fermilab [53].

use the two-component dual parton model in the form of DTUJET-93 [10].

B. Pion-proton and kaon-proton collisions

In the cosmic ray cascade beyond the first generation, the interactions of secondary hadrons, mainly pions and kaons, are as important or even more important than the interaction of nucleons. The dual parton model can be constructed for all hadronic projectiles. It is only required to know the flavors of the valence quarks in order to predict the hadron production by hadronic projectiles.

In this section we compare the hadron production in pion-proton and kaon-proton collisions as implemented in DPMJET-II with data in the fragmentation region.

In Figs. 18 and 19 we compare the model with the results of the EHS-NA22 experiment [45] at 250 GeV in $\pi^+ - p$ collisions. As in the corresponding comparisons with this experiment for p-p collisions, we find a satisfactory agreement of model and data. This refers to the produced π^- as well as to the leading π^+ mesons and to the diffractive peak in the leading particle distribution.

In Fig. 20 we compare at 175 GeV to data on $\pi^+ + p \to \pi^+ + X$ and $\pi^+ + p \to \pi^- + X$ from Brenner *et al.* [49]. In Fig. 21 we compare at 175 GeV to data on $K^+ + p \to K^+ + X$, $K^+ + p \to \pi^+ + X$, and $K^+ + p \to \pi^- + X$ from Brenner *et al.* [49]. In all of these comparisons we find a quite good agreement between the model and the data. We conclude that the dual parton model is able to describe hadron production in meson-nucleon collisions as well as in nucleon-nucleon collisions.

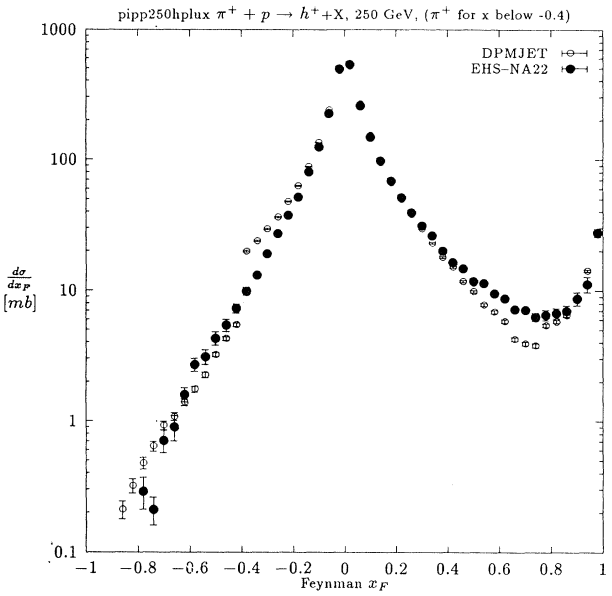

FIG. 19. Comparison of Feynman-x distributions of positively charged hadrons produced in π^+-proton collisions at 250 GeV. The experimental data are from the EHS-NA22 Collaboration [45]. For $x_F \leq -0.4$ the experimental and calculated distributions refer to π^+ only. The calculation uses the dual parton model DPMJET-II.

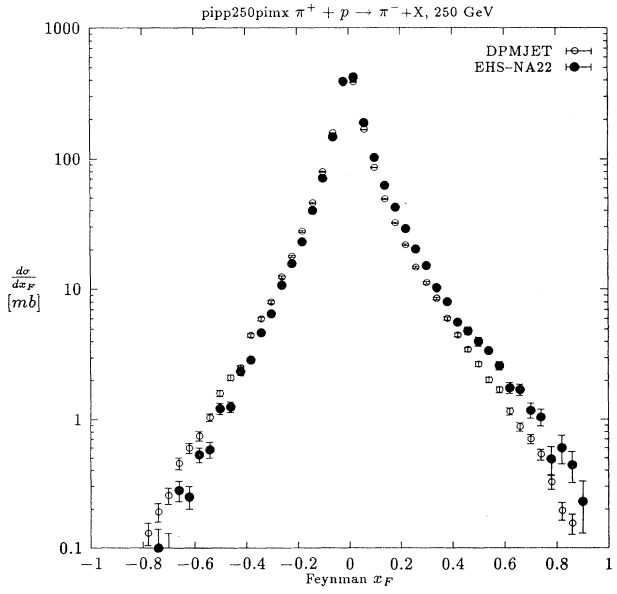

FIG. 18. Comparison of Feynman-x distributions of π^- mesons produced in π^+-proton collisions at 250 GeV. The experimental data are from the EHS-NA22 Collaboration [45]. The calculation uses the dual parton model DPMJET-II.

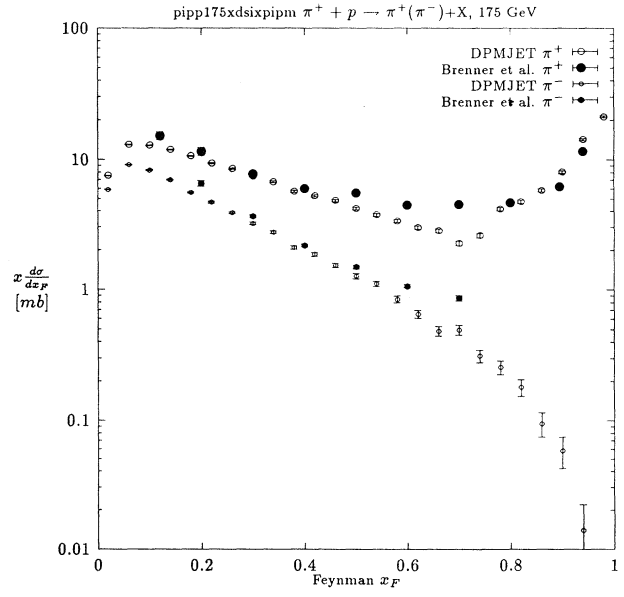

FIG. 20. Comparison of Feynman-x distributions of π^+ and π^- mesons produced in π^+-proton collisions at 175 GeV. The experimental data are from Brenner *et al.* [49]. The calculation uses the dual parton model DPMJET-II.

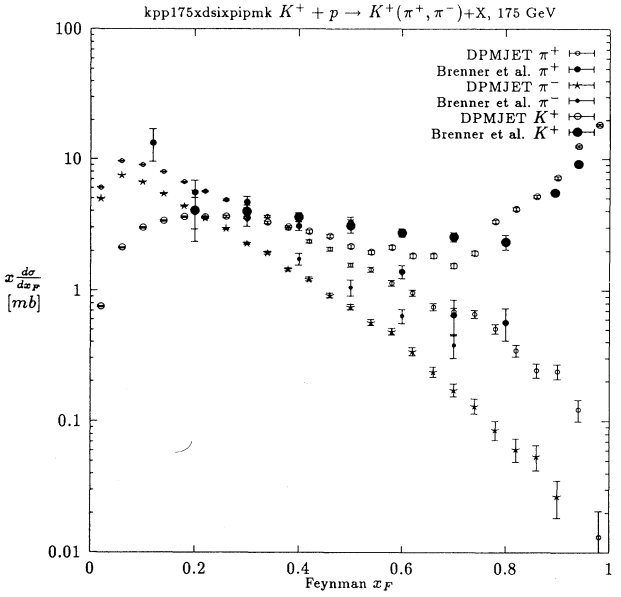

FIG. 21. Comparison of Feynman-x distributions of K^+, π^+, and π^- mesons produced in K^+-proton collisions at 175 GeV. The experimental data are from Brenner *et al.* [49]. The calculation uses the dual parton model DPMJET-II.

V. HADRON-NUCLEUS COLLISIONS WITH DPMJET-II

A. Hadron-air inelastic cross sections as function of the energy

The Glauber model, which is part of DPMJET-II, allows us to calculate the inelastic hadron-nucleus cross sections. What we need for this calculation is the nuclear geometry and the elementary hadron-nucleus scattering amplitude parametrized as follows.

Energy-dependent quantities enter the Glauber approach via the profile function of elastic hadron-nucleon scattering:

$$\gamma_{hN}(b) = \frac{1}{2\pi i p}\int d^2q \exp(i\mathbf{q}\cdot\mathbf{b}) f_{hN}(\mathbf{q}), \qquad (13)$$

i.e., the amplitude of elastic hadron-nucleon scattering in the impact parameter representation (with $\mathbf{q}$ denoting the lateral, i.e., two-dimensional momentum transfer). In their Monte Carlo realization of Glauber's approach Shmakov *et al.* [34] apply the high-energy approximation of the profile function:

$$\gamma_{hN}(b) = \frac{\sigma_{hN}^{\rm tot}}{4\pi a}\left(1 - i\frac{{\rm Re}f_{hN}(0)}{{\rm Im}f_{hN}(0)}\right)e^{-b^2/2a}, \qquad (14)$$

with parameters $\sigma^{\rm tot}$,a and $\rho = {\rm Re}f_{hN}(0)/{\rm Im}_{hN}(0)$ appropriate for the description of nucleus-nucleus interactions at energies of several GeV per nucleon. (This parametrization corresponds to a differential cross section $d\sigma/dt \simeq \sigma_{\rm tot}\exp(at)$ with $t \simeq -\bar{q}^2$.)

However, the energy dependence of the elastic hadron-nucleon scattering amplitudes will influence the properties of hadron-nucleus and nucleus-nucleus scattering. In particular, the number of individual high-energy hadron-nucleon interactions (n, n_A, n_B) will increase with rising energy, hence the multiplicity will increase stronger than to be expected from the energy dependence of single hadron-hadron interactions.

Guided by the data collected in Ref. [55], we apply the following parametrizations for the slope parameter a: $a = 8.5(1 + 0.065\ln s)$ for nucleon-nucleon collisions and $a = 6.0(1 + 0.065\ln s)$ for π- and K-nucleon collisions. We use for the ratio ρ of the real and imaginary part of the elastic scattering amplitude: $\rho = -0.63 + 0.175\ln\sqrt{s}$ for the energy region $3.0 \le \sqrt{s} \le 50$ and $\rho = 0.1$ in the energy region $\sqrt{s} \ge 50$ GeV in nucleon-nucleon scattering and $\rho = 0.01$ for π- and K-nucleon scattering. In models for the scattering amplitude (see Ref. [56]), the ratio ρ approaches zero at asymptotic energies; however, in the limited energy range ($\sqrt{s} \le 10$ TeV) where we present calculations in this paper, the constant value for ρ above 50 GeV is a rather good approximation to most of the models.

The energy dependence of the total cross sections is described by the fits of the Particle Data Group [57]; at energies beyond the range of the actual parametrization of the pp cross section the one for $\bar{p}p$ is applied and at energies even higher we use the total cross sections as calculated by the two-component dual parton model for hadron-hadron collisions [10].

The same information is also needed to construct the inelastic events and indeed usually each run of DPMJET starts with a calculation of the inelastic cross section.

In Fig. 22 we compare the p-air cross sections calcu-

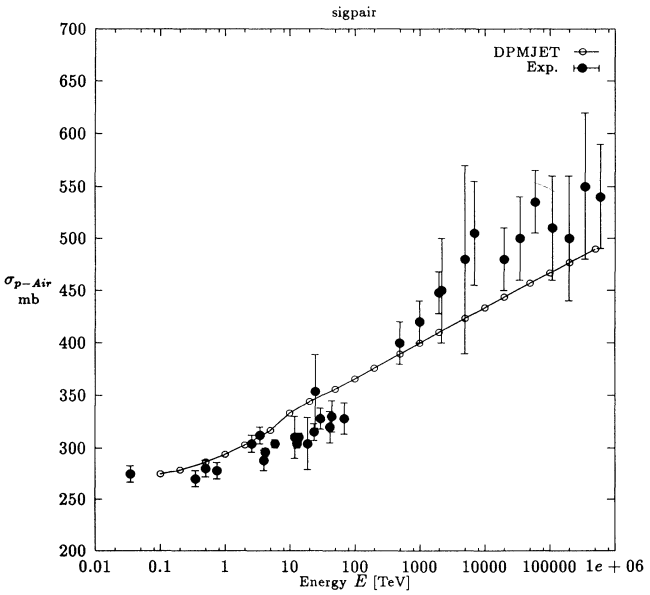

FIG. 22. The total cross section $\sigma_{p\text{-Air}}$ as function of the collision energy as calculated using the Glauber model in DPMJET-II. The calculation is compared to cosmic ray data collected by Mielke *et al.* [74].

lated with DPMJET-II to data form cosmic ray experiments.

B. Feynman scaling in hadron-nucleus collisions

In order to understand the relevance of accelerator data on particle production in hadron-nucleus collisions for the cosmic ray cascade, we study again the Feynman scaling behavior of p+air$\rightarrow \pi^+ + X$. This is done in Fig. 23, where we plot the $x_F dN/dx_F$ distributions for laboratory energies of 1, 10, 100, and 1000 TeV. As above in proton-proton collisions, we find again that Feynman scaling is very well satisfied in most of the x_F region. Exceptions are again the region around $x_F = 0$, where the rise of the rapidity plateau violates Feynman scaling, and the region $x_F = 1$ for leading particles, where the diffractive component does not show Feynman scaling. Given this Feynman scaling behavior, we can again conclude that accelerator data and their agreement to the model are indeed very relevant to the cosmic ray application of the model.

C. Feynman x distributions in collisions of protons with light nuclei and the $\alpha(x_F)$ behavior

In Fig. 24 we compare at 400 GeV the Feynman x_F distributions of produced protons and π^+ mesons in proton-proton, proton-beryllium, proton-air, proton-aluminium, and proton-copper collisions as calculated with DPMJET-II. We observe in the relevant x_F region the x_F distributions from p-p to p-Air to differ by less than a factor of 2 and the distributions changing the target from p-Be over p-air to p-Al again to change by less than a factor of 2. The latter change can be described by $\alpha(x_F)$, representing the cross section as

$$x_F \frac{d\sigma^{p-A}}{dx_F} = A^{\alpha(x_F)} x_F \frac{d\sigma^{p-N}}{dx_F}. \qquad (15)$$

For the transition p-p to p-air this $A^{\alpha(x_F)}$ behavior is not relevant, since we know that this kind of extrapolating h-A total cross sections to p-p does not give the correct p-p total cross section. Usually $\alpha(x_F)$ is determined using data for two or more different target nuclei without ever considering p-N collisions.

The x_F distributions for p-p and p-air collisions in Fig. 24 cross in the region below $x_F = 0.2$. This crossing diminishes further the errors, which can result from errors in the p-p to p-air transition. Unfortunately, there are no precise data (from the same experiment) where the differences of Feynman x_F distributions in p-p and p-light nucleus collisions could be checked. Therefore, for this transition, the best we can do at present is to rely on the model.

We do not learn much more, if we compare to experiment, where the hadron production on light target materials is measured in the form of double differential distributions. Such comparisons were done. The errors in such a double differential comparison are usually rather big and difficult to understand.

The results of double differential cross sections for inclusive hadron production in hadron-nucleus collisions have been represented in the form

$$E\frac{d^3\sigma^{p-A}}{d^3p} = A^{\alpha(x_F,p_\perp)} E\frac{d^3\sigma^{p-N}}{d^3p}. \qquad (16)$$

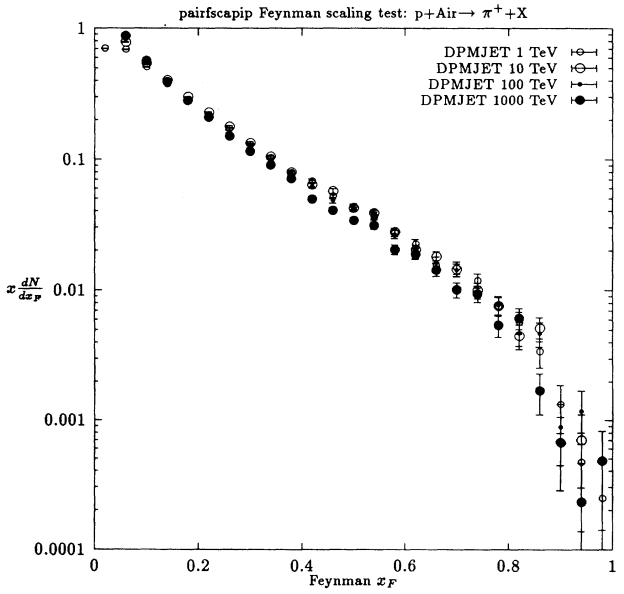

FIG. 23. Test of Feynman scaling in the production of π^+ in proton-air collisions. The Feynman-x distributions were calculated with the dual parton model DPMJET-II.

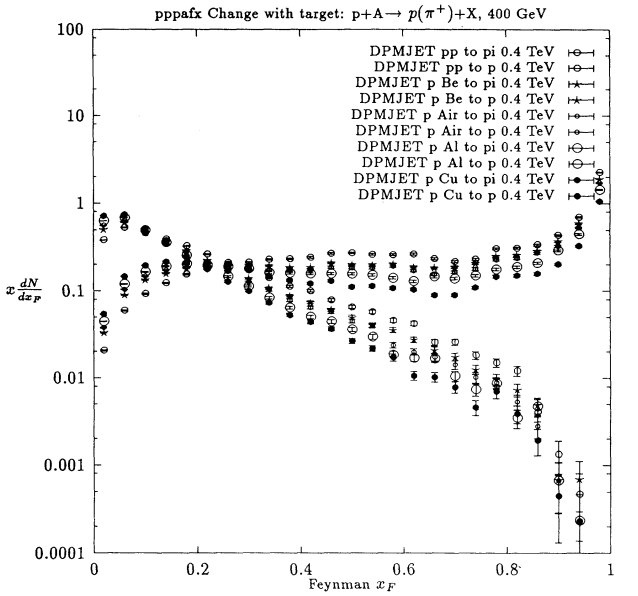

FIG. 24. Change of the Feynman-x distributions of protons and π^+ mesons produces in 400 GeV collisions with the mass of the target nucleus. The calculation uses the dual parton model DPMJET-II.

With data on two different target nuclei, one can extract $\alpha(x_F, p_\perp)$ without the knowledge of $Ed^3\sigma/d^3p^{p-N}$. The data of Barton *et al.* [58] at 100 GeV and at a transverse momentum $p_\perp = 0.3$ GeV/c were used to get $\alpha(x_F)$ (in reality: $\alpha(x_F, p_\perp = 0.3$ GeV/$c)$). In the Monte Carlo calculation it is difficult to get such a good statistics at fixed $p_\perp$, to extract meaningful $\alpha(x_F)$ values. This is just possible for single differential distributions in x_F. In Fig. 25 we compare the $\alpha(x_F)$ as obtained by Barton *et al.* [58] for pion production at $p_\perp = 0.3$ GeV/c with $\alpha(x_F)$ obtained from DPMJET-II results for all charged hadrons integrated over all $p_\perp$. The model results have been obtained using 1.5 million events for each of the four reactions considered, even with this statistics the errors are still large and it is not possible to compute the α values for only one $p_\perp$ bin. The agreement in the x_F region of overlap is reasonable. For $x_F \to 0$ in the dual parton model the limiting $\alpha(x_F)$ value is 1. This is actually also obtained from DPMJET-II. For large values of x_F the limiting $\alpha(x_F \to 1)$ for the data as well as for the Monte Carlo calculation seems to be around 0.4.

The agreement with these $\alpha(x_F)$ data is the strongest point for the claim that the dual parton model in the form of the DPMJET-II event generator gives a good description of the nuclear dependence of hadron production in the fragmentation region. We stress, however, once again, these $\alpha(x_F)$ data are only for fixed $p_\perp$ and it would be highly desirable to obtain better data for the change of hadron production from proton-proton collisions to collisions of protons with light target nuclei.

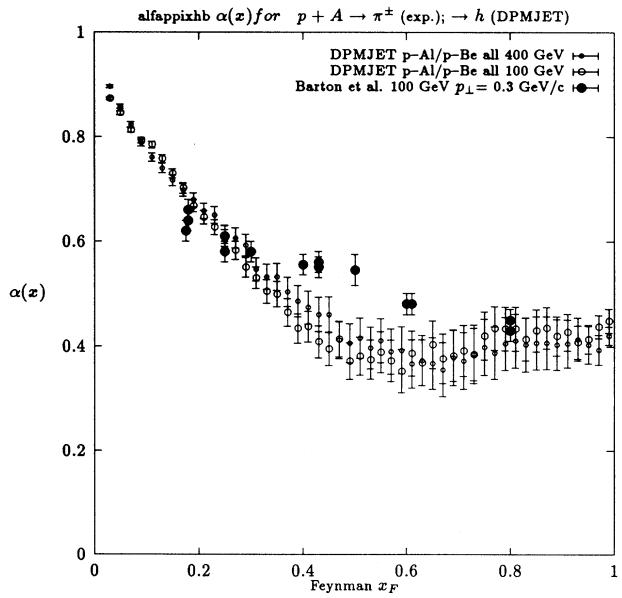

FIG. 25. The nuclear dependence of the Feynman-x distribution in hadron-nucleus collisions is represented in the form $d\sigma/dx_{h-A} = A^{\alpha(x)} d\sigma/dx_{h-h}$. We compare $\alpha(x)$ as determined by Barton *et al.* [58] for pion production at $p_\perp = 0.3$ GeV/c with the DPMJET-II results for all charges hadrons at all values of $p_\perp$.

D. Transverse momentum distributions in hadron-nucleus collisions, transverse momentum ratios, and the $\alpha(p_\perp)$ behavior

In Figs. 26 and 27 we compare transverse momentum distributions calculated with DPMJET-II for p-W and p-Au collisions at 200 GeV with data [59] and [60] and find a good agreement.

In order to show the changes in the transverse momentum distributions from p-p to p-A collisions, one presents the data in the form of $p_\perp$ ratios

$$R(p_\perp) = \frac{E\frac{d^3N^{p-A}}{d^3p}}{E\frac{d^3N^{p-p}}{d^3p}}, \tag{17}$$

or one uses the $\alpha(p_\perp)$ representation

$$E\frac{d^3\sigma^{p-A}}{d^3p} = A^{\alpha(p_\perp)} E\frac{d^3\sigma^{p-N}}{d^3p}. \tag{18}$$

In Fig. 28 we compare DPMJET-II with $\alpha(p_\perp)$ data from Garbutt *et al.* [61]. The data are for identified kinds of secondary hadrons. In the model calculation we present $\alpha(p_\perp)$ only for π^+ and K^+. Again, we use 1.5 million Monte Carlo events for each reaction used to generate this plot. We find a rather good agreement with the data for π^+. The $\alpha(p_\perp)$ calculated for K^+ are systematic above the values for π^+, but they stay in the region with good statistics below the data for the K^+.

In Fig. 29 we present how the seagull effect as calculated in DPMJET-II for p-air collisions scales with energy. The calculations are at energies between 1 TeV and 1000 TeV. At all energies $\langle p_\perp(x_F)\rangle$ rises significantly with x_F (at least in the region $x_F \leq 0.5$.) At the same time the average transverse momentum rises at all x_F values

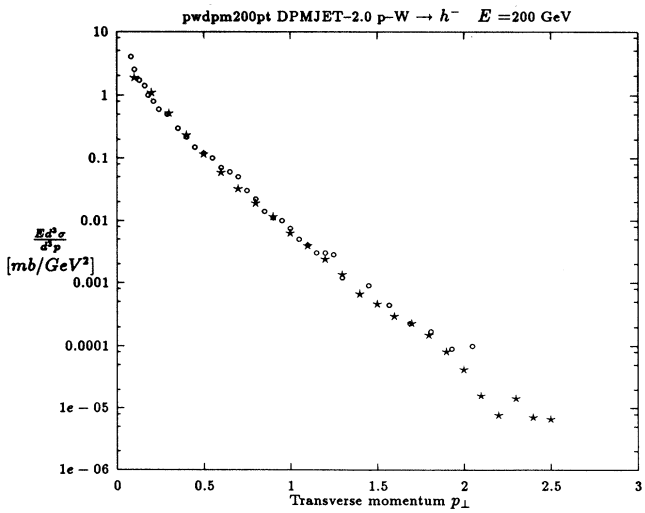

FIG. 26. Transverse momentum distribution of negatively charged hadrons in p-W collisions at the energy of 200 GeV. We compare the data from the HELIOS Collaboration [59] with the distribution from the dual parton model DPMJET-II.

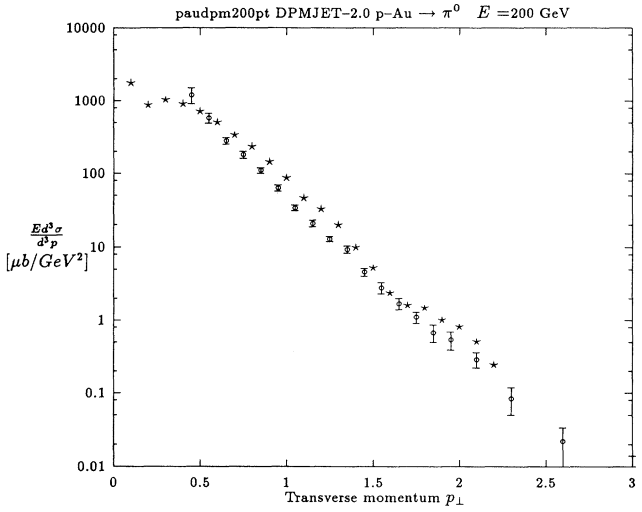

FIG. 27. Transverse momentum distribution of π^0 mesons in p-Au collisions at the energy of 200 GeV. We compare the data from the WA80 Collaboration [60] with the distribution calculated from the dual parton model DPMJET-II.

strongly with the collision energy. This rise in the model is mainly due to the rise of minijet production and due to the Cronin effect in the nuclear target.

E. Production of strange particles in hadron-nucleus collisions

Some important questions for cosmic ray studies are the following: (i) Is there an enhancement of strange particle production if we go at the same energy from proton-proton to proton-nucleus collisions? (ii) Does the strange hadron production in hadron-nucleus collisions rise faster than the inelastic cross section, or does the multiplicity ratio $n_{\text{strange}}/n_{\text{nonstrange}}$ increase with the mass A of the target nucleus?

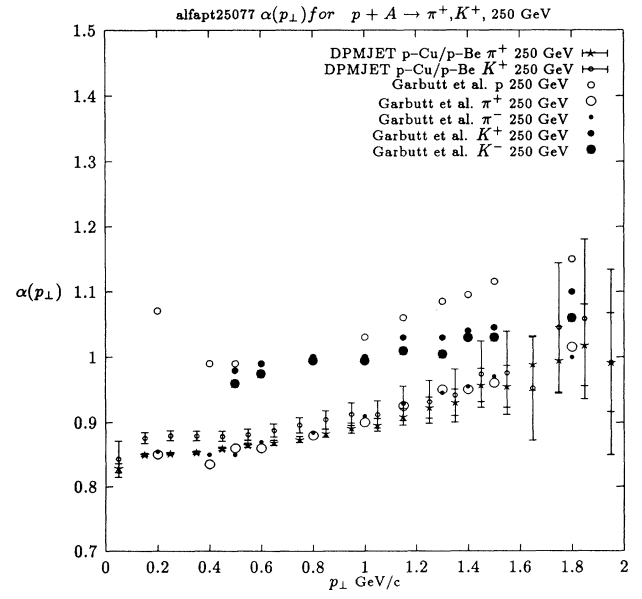

FIG. 28. The nuclear dependence to the $p_\perp$ distributions in proton-nucleus collisions is represented in the $A^{\alpha(p_\perp)}$ form. We compare data from Garbutt *et al.* [61] for different kinds of produced particles with the results of the dual parton model DPMJET-II for π^+ and K^+.

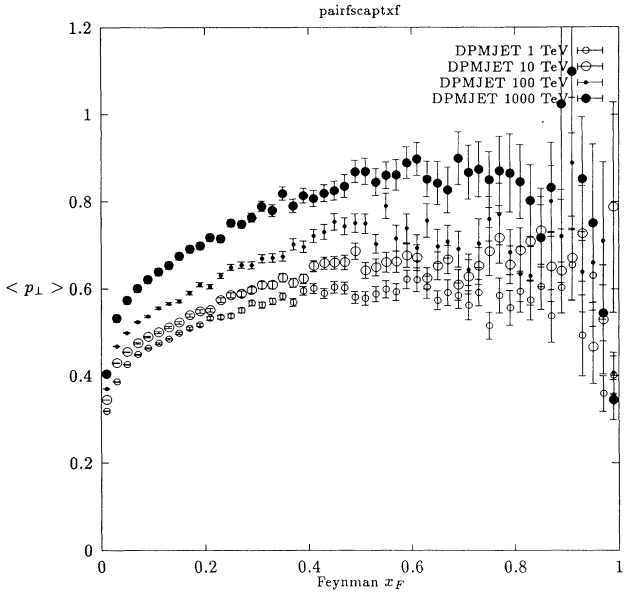

FIG. 29. The seagull effect as calculated from DPMJET-II for proton-air collisions at energies between 1 and 1000 TeV.

One can look at multiplicities of strange and nonstrange hadrons from some experiments (such data were collected by Bialkowska *et al.* [62]). A look at such a compilation shows that the statistical and systematical uncertainties of the data do not allow us to draw any conclusion about a systematic increase or decrease.

Fortunately, there are some experiments where the strange and nonstrange hadron production on different target nuclei are compared in the form A^α, and α values are given separately for strange and nonstrange produced hadrons. We review the results of three of these experiments.

(i) Antreasyan *et al.* [52] measure the *Cronin effect.* They present (in their Fig. 16) $\alpha_K - \alpha_\pi$ as function of $p_\perp$ and find it to be larger than zero at all measured $p_\perp$ values. This means that the K/π ratio increases with A. Unfortunately, their lowest $p_\perp$ value is 0.77 GeV/c (where $\alpha_K - \alpha_\pi$ is around 0.07) and one might doubt whether this allows a conclusion about all of the low-$p_\perp$ particle production.

(ii) An experiment similar to the one of Antreasyan *et al.* [52] was performed by Garbutt *et al.* [61], (see also Fig. 28) fortunately at $p_\perp$ values between 0.2 and 2.4 GeV/c. Here also, at all $p_\perp$ they find $\alpha_K - \alpha_\pi \approx 0.1$. In DPMJET-II we find $\alpha_{K^+} - \alpha_{\pi^+}$ systematically larger than zero, but smaller than 0.1. Again, from the data as well as from the model, the conclusion is that K/π increases systematically with A.

(iii) Skubic *et al.* [63] present α values as function of Feynman x_F and $p_\perp$ for K^0_S production at 300 GeV. α values are given for $x_F = 0.2$, 0.4, and 0.6 and $p_\perp$ values between 0 and 1.5 GeV/c. At $p_\perp$ values below 0.8 GeV/c, all $\alpha(x_F, p_\perp)$ are found smaller than $\frac{2}{3}$, but $\alpha(x_F, p_\perp)$ increases with decreasing x_F, and we might hope that in the x_F region around 0 (from where the dominant $K^\pm$ and K^0 production come) again $\alpha(x_F, p_\perp)$ will be found bigger than 2/3. A modest rise of the K/π ratios with the mass of the target nucleus is also found in DPMJET-II; it is, however, difficult to get enough statistics to extract meaningful α values from the Monte Carlo calculation.

VI. NUCLEUS-NUCLEUS COLLISIONS

A. Nucleus-air inelastic cross sections as function of the energy

The same Glauber model, which gives the hadron-air inelastic cross sections is also able to calculate nucleus-nucleus inelastic cross sections. In Fig. 30 we present nucleus-air inelastic cross sections calculated with DPMJET-II in the energy range 0.1 TeV to 10^7 TeV. All these cross sections rise with the energy, but the relative rise of the cross sections from the lowest to the highest energy is smaller for heavy projectiles, since in the center, at small impact parameters the nuclei become black already at lower energies.

B. Comparison of nucleus-nucleus collisions according to DPMJET-II with the superposition model

Instead of the proper sampling of nucleus-nucleus scattering events, an approximation often applied is the so-called superposition model. There are two different possible superposition models: (i) a nucleus-nucleus collision A-B with N_p participating projectile nucleons is approximated as the superposition of N_p simultaneous nucleon-nucleon collisions; (ii) a nucleus-nucleus collision A-B with N_p participating projectile nucleons is approximated as the superposition of N_p simultaneous nucleon-B collisions. In Tables II and III we present multiplicities and spectrum-weighted moments calculated using DPMJET-II for C-air collisions. The comparisons in these two tables with both versions of the superposition model show that the superposition is only a very rough and unreliable approximation to real nucleus-nucleus collisions.

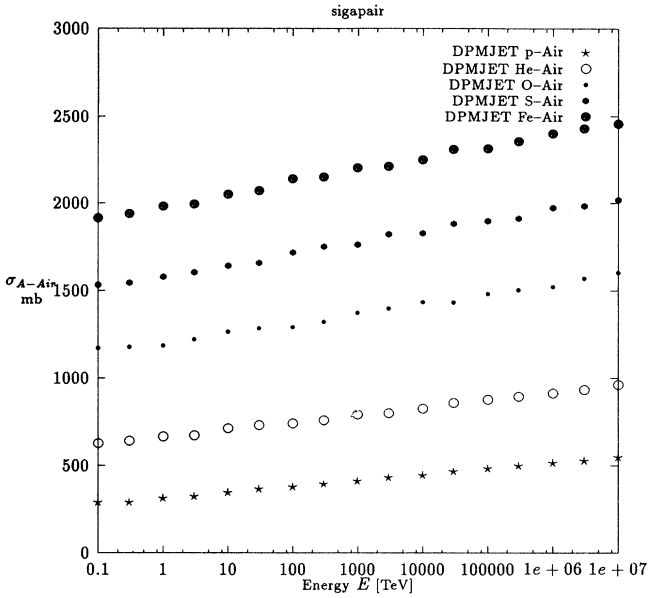

FIG. 30. Total nucleus-air cross sections $\sigma_{A\text{-Air}}$ as function of the collision energy as calculated using the Glauber model in DPMJET-II.

VII. DPMJET-II AT COSMIC RAY ENERGIES

In [64] we will report about the application of DPMJET-II to study the cosmic ray cascade. Here we give only some general properties of DPMJET-II in this energy range.

A. Important differences between the two-component dual parton model and minijet models

There is no scientific reason not to call the two-component dual parton model (the two components are the soft pomeron and the hard pomeron or the minijets) also a minijet model. Minijet models too have soft and a hard components. The reason not to use the term minijet model for DPMJET is connected with the fact that the name minijet model so far was only used for models which use a critical Pomeron with an intercept of exactly one. In such a minijet scheme, it is then claimed, all the rise of the cross sections with energy is due to the rise of

TABLE II. Comparison of average multiplicites calculated in C-air collisions at different energies with the expectations in two different superposition models. N_p is the average number of projectile nucleons taking part in the inelastic C-air collision. The energies given are the energy per nucleon.

Energy (TeV)	N_p	$n_{\pi^+}^{C\text{-air}}$	$n_{\pi^+}^{p\text{-}p}$	$n_{\pi^+}^{p\text{-air}}$	$N_p n_{\pi^+}^{p\text{-}p}$	$N_p n_{\pi^+}^{p\text{-air}}$
10	4.21	27.96	4.35	6.76	18.31	28.46
100	4.45	46.89	6.56	11.35	29.19	50.51
1000	4.69	73.71	9.31	17.45	43.66	81.84

TABLE III. Comparison of Z_π moments calculated in C-air collisions at different energies with the expectations in two different superposition models. N_p is the average number of projectile nucleons taking part in the inelastic C-air collision. The energies given are the energy per nucleon.

Energy (TeV)	N_p	$Z_\pi^{C\text{-air}}$	$Z_\pi^{p\text{-}p}$	$Z_\pi^{p\text{-air}}$	$N_p Z_\pi^{p-p}$	$N_p Z_\pi^{p\text{-air}}$
10	4.21	0.3619	0.076	0.067	0.3200	0.2821
100	4.45	0.3778	0.076	0.069	0.3382	0.3071
1000	4.69	0.3872	0.076	0.068	0.3564	0.3189

TABLE IV. Z_π and Z_K moments and leading baryon elasticities or average energy fractions K_{ln} in p-p and p-air collisions.

Collision Energy (TeV)	p-p Z_π	p-p Z_K	p-p K_{ln}	p-air Z_π	p-air Z_K	p-air K_{ln}
0.2	0.077	0.0094	0.45			
0.4	0.076	0.0092	0.45			
1	0.076	0.0093	0.45	0.067	0.0098	0.37
10	0.076	0.0092	0.44	0.069	0.0099	0.33
100	0.076	0.0095	0.42	0.068	0.0102	0.31
1000	0.075	0.0093	0.40	0.066	0.0101	0.27

TABLE V. Z_π and Z_K moments in $\pi^+ - p$ and π^+-air collisions.

Collision Energy (TeV)	π^+-p Z_π	π^+-p Z_K	π^+-air Z_π	π^+-air Z_K
0.2	0.26	0.019	0.24	0.018
1	0.27	0.018	0.23	0.017
10	0.27	0.018	0.23	0.016
100	0.26	0.018	0.21	0.016
1000			0.19	0.015

TABLE VI. Z_π and Z_K moments in K^+-p and K^+-air collisions.

Collision Energy (TeV)	K^+-p Z_π	K^+-p Z_K	K^+-air Z_π	K^+-air Z_K
0.2	0.093	0.171	0.082	0.156
1	0.092	0.181	0.084	0.156
10	0.091	0.188	0.082	0.145
100	0.086	0.183	0.080	0.132
1000			0.076	0.113

the minijet cross sections. This is not so in our model, therefore we avoid using the name minijet model.

The supercritical Pomeron was used in the two-component DPM from the beginning [4], while the so-called minijet models use the critical Pomeron with $\alpha(0) = 1$ from Durand and Pi [65] over Gaisser and Halzen [66], SIBYLL [67] up to HIJING [68].

There are important differences which result from this different approach.

(i) Both kinds of models determine the free parameters of their model in a fit to total, inelastic and elastic cross sections. Both models obtain acceptable fits; we have reported even about the fits using a critical Pomeron elsewhere [8], but of course, if at the end of the fit we treat the Pomeron intercept $\alpha(0)$ as a free parameter instead of fixing it to $\alpha(0) = 1$, the fit improves and in all situations (fits using different parton structure functions to calculate the minijet cross sections) we obtain the intercept larger than 1, namely, $\alpha(0) \approx 1.07$. These better fits to the data are our main argument for the continuing presence and even rise of soft hadron production at the highest energies.

(ii) Because of these different starting points the chain structure of the models differ: In both models we have a pair of soft valence-valence chains (resulting from cutting one soft Pomeron) and in both models we have minijets. Only in the two-component dual parton model do we have in addition soft sea-sea chains with soft sea quarks at their ends. The number of these chains increases with energy and a substantial part of the rise of the multiplicity and rapidity plateau results from this mechanism.

(iii) The x distributions of soft sea quarks are determined by the Regge behavior, which is for soft sea as well as valence quarks like $1/\sqrt{(x)}$. The minijets are calculated from the deep inelastic structure functions with (depending on the parametrization for the structure functions used) a behavior such as $1/x$ or $1/x^{1.5}$. In the dual parton model the Feynman x_F distributions resulting from fragmenting valence chain ends (which dominate at small energy) and from fragmenting soft sea chain ends to not differ; this is the source of the excellent Feynman scaling and the nearly energy independent spectrum weighted moments. In the minijet models all chains except the single valence chain pair, which dominates at low energy, are minijets with the much softer x distribution. Therefore in these models Feynman scaling is more strongly violated and the spectrum weighted moments decrease with the collision energy. The rise of the minijet component in the dual parton model leads of course to the same effect. This effect is, however, smaller, since not all of the rise of particle production is due to the minijets.

B. Spectrum-weighted moments

In Table IV we present spectrum-weighted moments Z_π and Z_K according to DPMJET-II in p-p and p-air collisions and elasticities for the leading baryon K_{ln} (K_{ln} is defined as the average energy fraction carried by the single most energetic baryon in each event). We find, as explained already in the preceding section, Z_π and Z_K moments rather constant with the collision energy. The moments for p-air collisions are smaller than for p-p collisions. This decrease is connected with the $\alpha(x_F)$ behavior as given in Fig. 25. The elasticities K_{ln} decrease with energy; this decrease will be discussed in the next section.

In Tables V and VI we give Z_π and Z_K moments in π^+-p, π^+-air, K^+-p and K^+-air collisions. Again, the moments for the produced particles are rather constant with rising energy, while the moments for the leading hadrons decrease systematically with rising energy.

In Table VII we compare the Z_π and Z_K moments calculated with DPMJET-II in p-air collisions with the ones resulting from HEMAS [69] (the actual numbers given result from a recent version of the HEMAS code [70]) and SIBYLL [67]. The agreement of the moments, especially the ones from DPMJET-II and from SIBYLL is certainly much better, than expected from the errors of the experimental data used to tune the parameters of the models.

C. Average energy fractions

In Table IV we presented already the elasticities K_{ln} for leading baryons as calculated from DPMJET-II for p-p and p-air collisions. In Table VIII we present the average energy fractions K_h carried by secondary hadrons of kind h in p-air collisions as calculated from DPMJET-II for the most important secondaries as function of the energy.

We observed in Tables IV and VIII a decrease with energy of the average energy fractions of all leading baryons (p, n, and Λ), while the average energy fractions of all newly produced kinds of hadrons increase with energy. A large part of this effect is due to the diffractive component.

In the two-component dual parton model [10] we obtain inelastic cross sections rising with energy like $\ln^2 s$. The single diffractive cross sections, where the experimental data are not really a guidance, seem in the model at high energy to approach an energy independent value. A similar result was obtained recently by Gotsman, Levin, and Maor [71]. The double diffractive cross sections in the model behave similarly.

The average energy fractions of leading hadron are particularly large in diffractive events. If the relative fraction of diffractive events decreases with rising energy, we expect a decrease of the average energy fractions of the leading hadrons and a corresponding increase of the average energy fractions of produced hadrons as found in Table VIII. In this situation, we stress the importance of experimental measurements of the hadron production in the fragmentation region, including the measurement of diffractive cross sections at the highest available accelerator energies at the Fermilab Collider. Without such experimental data we have only the models to extrapolate into the cosmic ray energy region.

TABLE VII. Comparison of Z_π and Z_K moments in p-air collisions between DPMJET-II, HEMAS [69] (the actual numbers given result from a recent version of the HEMAS code [70]), and SIBYLL [67].

Energy (TeV)	DPMJET Z_π	HEMAS Z_π	SIBYLL Z_π	DPMJET Z_K	HEMAS Z_K	SIBYLL Z_K
1	0.067	0.061	0.072	0.0098	0.0104	0.0073
10	0.069	0.057	0.068	0.0099	0.0113	0.0071
100	0.068	0.056	0.067	0.0102	0.0116	0.0070
1000	0.066	0.056	0.066	0.0101	0.0123	0.0070

D. Upper energy limit for DPMJET-II calculations

Presently DPMJET-II is able to run up to energies of approximately 10^{18} eV in the lab system. There are trivial reasons for this limit (dimensions in fields to be defined during initialization), which could result in a failure to run at higher energies. Such problems would be easy to solve, but there are besides these trivial reasons physical reasons that the code should not be used at higher energies.

The most important of these reasons is connected with the minijet component. The way in which the minijet component is implemented in DTUJET-93 and DPMJET-II is described in Ref. [10]. This method is expected to break down for structure functions with $1/x^{1.5}$ singularities (for sea quarks and gluons) at higher energies. These structure functions are suggested by the first measurements at the HERA accelerator. For the older structure functions with a $1/x$ singularities, it would be rather straightforward to define the minijet component at higher energies, but this might not correspond to the correct physics. There are certainly ideas how to extend the treatment of the minijet component up to higher energies, but this would be connected with large and extensive modifications in the model.

VIII. SUMMARY

The event generator DPMJET-II based on the dual parton model has become a valid alternative to models such as HEMAS [69] and SIBYLL [67] to simulate the high energy hadron-hadron, hadron-nucleus, and nucleus-nucleus collisions within a cosmic ray cascade code.

The excellent Feynman scaling found with DPMJET in large parts of the x_F region in hadron-hadron and hadron-nucleus collisions gives us the confidence that accelerator data on Feynman x_F distributions in the projectile fragmentation region are indeed very relevant for applications in the cosmic ray energy region.

The model provides hadron-hadron total, inelastic, elastic, and diffractive cross sections consistent with accelerator data. The hadron-air cross sections derived from this are consistent with hadron-air cross sections extracted from cosmic ray experiments. The model also provides all the necessary cross sections to study nucleus-nucleus collisions in the cosmic ray cascade.

As a consequence of the excellent Feynman scaling in the model, we find spectrum-weighted moments Z_π and Z_K for hadron-air collisions, which remain rather constant with increasing collision energy, in contrast to the behavior of other models, where these moments decrease more strongly with energy. These moments for h-air collisions, however, are smaller than the corresponding moments in hadron-hadron collisions.

The fraction of the primary energy carried by the leading particles in the collision decreases with energy and with the mass of the target nuclei. A large part of this decrease is due to the decreasing fraction of diffractive (single diffractive and double diffractive) events with rising energy and rising target mass.

The model incorporates the Cronin effect and shows a strong seagull effect. Correspondingly, the average transverse momenta $\langle p_\perp \rangle$ rise with the collision energy (mainly due to the rise of the minijet production cross section), with the mass of the nuclear target and projectile and with rising Feynman x_F.

It is important that the model is able to give a good description of hadron production in nucleus-nucleus collisions. Because of large fraction of nuclei in primary cosmic rays nucleus-air collisions are of great importance in the cosmic ray cascade. It has been shown that these collisions in the dual parton model differ from what is expected in simple approximations such as different superposition models.

Finally, we find, in agreement with what is known

TABLE VIII. Average energy fractions K_h in p-air collisions as calculated with DPMJET-II. Please note that the K_h do not add up to 1.0 since most hyperons and antihyperons as well as antineutrons are not included in the table.

Energy [TeV]	K_p	$K_{\bar{p}}$	K_n	$K_{\pi+}$	$K_{\pi-}$	K_{K+}	K_{K-}	K_Λ	K_{π^0}	$K_{K^0_S+K^0_L}$
1	0.265	0.011	0.093	0.167	0.138	0.024	0.018	0.023	0.174	0.041
10	0.233	0.012	0.091	0.175	0.147	0.025	0.020	0.022	0.181	0.044
100	0.212	0.013	0.088	0.179	0.154	0.026	0.022	0.022	0.185	0.046
1000	0.189	0.014	0.083	0.185	0.162	0.027	0.023	0.021	0.191	0.049
10 000	0.168	0.015	0.077	0.190	0.169	0.029	0.025	0.020	0.198	0.052
100 000	0.152	0.016	0.075	0.194	0.173	0.029	0.026	0.020	0.201	0.054

from accelerator experiments, significant enhancements of strange hadron production with the collision energy, with the transverse momentum, with the secondary multiplicity of the collision and with the mass of the nuclear projectiles and targets.

ACKNOWLEDGMENTS

The author acknowledges collaboration with P. Aurenche, F. Bopp, A. Capella, R. Engel, A. Ferrari, H. J. Möhring, C. Pajares, D. Pertermann, S. Roesler, P. Sala, and J. Tran Thanh Van on different aspects of the dual parton model. The collaboration with G. Battistoni and C. Forti on different aspects of the cosmic ray application of the model was essential for the progress of the studies presented. The author acknowledges the hospitality of Professor L. Mandelli in Milano and Professor E. Iarocci and Professor M. Spinetti in Frascati, where the presented calculations were performed and he thanks INFN for supporting these studies.

[1] G. F. Chew and C. Rosenzweig, Nucl. Phys. **B104**, 290 (1976).
[2] C. Hong-Mo, J. E. Paton, and T. Sheung Tsun, Nucl. Phys. **B86**, 470 (1975).
[3] A. Capella, U. Sukhatme, Chung I Tan, and J. Tran Thanh Van, Phys. Rep. **236**, 225 (1994).
[4] A. Capella, J. Tran Thanh Van, and J. Kwiecinski, Phys. Rev. Lett. **58**, 2015 (1987).
[5] P. Aurenche, F. W. Bopp, A. Capella, J. Kwiecinski, M. Maire, J. Ranft, and J. Tran Thanh Van, Phys. Rev. D **45**, 92 (1992).
[6] F. W. Bopp, A. Capella, J. Ranft, and J. Tran Thanh Van, Z. Phys. C **51**, 99 (1991).
[7] F. W. Bopp, D. Pertermann, and J. Ranft, Z. Phys. C **54**, 683 (1992).
[8] R. Engel, F. W. Bopp, D. Pertermann, and J. Ranft, Phys. Rev. D **46**, 5192 (1992).
[9] S. Roesler, R. Engel, and J. Ranft, Z. Phys. C **59**, 481 (1993).
[10] F. W. Bopp, D. Pertermann, R. Engel, and J. Ranft, Phys. Rev. D **49**, 3236 (1994).
[11] B. L. Combridge, J. Kripfganz, and J. Ranft, Phys. Lett. **70B**, 234 (1977).
[12] K. Hahn and J. Ranft, Phys. Rev. D **41**, 1463 (1990).
[13] A. Capella and J. Tran Thanh Van, Z. Phys. C **10**, 249 (1981).
[14] A. B. Kaidalov and O. I. Piskunova, Z. Phys. C **30**, 145 (1986).
[15] A. D. Martin, R. G. Roberts, and W. J. Stirling, Phys. Rev. D **47**, 867 (1993).
[16] C.-C. J. Botts *et al.*, Phys. Lett. B (to be published).
[17] E. M. Levin, *QCD-20 Years Later*, Proceedings of the Workshop, Aachen, Germany, 1992, edited by P. M. Zerwas and H. A. Kastrup (World Scientific, Singapore, 1993).
[18] I. Abt *et al.*, Nucl. Phys. **B407**, 515 (1993).
[19] J. Kwiecinski, A. D. Martin, R. G. Roberts, and W. J. Stirling, Phys. Rev. D **42**, 3645 (1990).
[20] J. Ranft and S. Ritter, Z. Phys. C **20**, 347 (1983).
[21] J. Ranft and S. Ritter, Z. Phys. C **27**, 569 (1985).
[22] H.-J. Möhring, J. Ranft, and S. Ritter, Z. Phys. C **27**, 419 (1985).
[23] J. Ranft, Phys. Lett. B **188**, 379 (1987).
[24] J. Ranft, Z. Phys. C **43**, 439 (1989).
[25] V. S. Barashenkov and V. D. Toneev, *High-Energy Hadron-Nucleus and Nucleus-Nucleus Interactions* (in Russian) Atomisdat, Moscow, 1972.
[26] H. W. Bertini, Phys. Rev. **131**, 1801 (1963).
[27] L. Landau and I. Pomeranchuk, Dokl. Akad. Nauk SSR **92**, 535 (1953); **92**, 734 (1953).
[28] L. Stodolski, *Proceedings of the Vth Intern. Colloquium on Multiparticle Reactions* (Oxford University Press, New York, 1975), p. 577.
[29] J. Ranft, Phys. Rev. D **37**, 1842 (1988).
[30] H.-J. Möhring and J. Ranft, Z. Phys. C **52**, 643 (1991).
[31] I. Kawrakow, H.-J. Möhring, and J. Ranft, Z. Phys. C **56**, 115 (1992).
[32] H.-J. Möhring, J. Ranft, A. Capella, and J. Tran Thanh Van, Phys. Rev. D **47**, 4146 (1993).
[33] J. Ranft, A. Capella, and J. Tran Thanh Van, Phys. Lett. B **320**, 346 (1994).
[34] S. Yu. Shmakov, V. V. Uzhinskii, and A. M. Zadoroshny, Comput. Phys. Commun. **54**, 125 (1989).
[35] S. Ritter, Comput. Phys. Commun. **31**, 393 (1984).
[36] J. Ranft and S. Ritter, Acta Phys. Pol. B **11**, 259 (1980).
[37] K. Hänssgen and S. Ritter, Comput. Phys. Commun. **31**, 411 (1984).
[38] T. Sjöstrand, CERN Report No. CERN-TH.6488/92, 1992 (unpublished).
[39] J. W. Cronin *et al.*, Phys. Rev. D **11**, 3105 (1975).
[40] H. R. Schmidt and J. Schukraft, GSI Report No. GSI-92-19, 1992 (unpublished).
[41] S. Roesler and J. Ranft, Z. Phys. C **62**, 336 (1994).
[42] I. Kawrakow, H.-J. Möhring, and J. Ranft, Phys. Rev. D **47**, 3849 (1993).
[43] H.-J. Möhring and J. Ranft, Z. Phys. C **52**, 643 (1991).
[44] M. Gazdzicki and O. Hansen, Nucl. Phys. **A528**, 754 (1991).
[45] EHS-NA22 Collaboration, M. Adamus *et al.*, Z. Phys. C **39**, 311 (1988).
[46] LEBS-EHS Collaboration, M. Aguilar-Benitez *et al.*, Z. Phys. C **50**, 405 (1991).
[47] EHS-RCBC-Collaboration, J. L. Bailly *et al.*, Z. Phys. C **35**, 309 (1987).
[48] T. Kafka *et al.*, Phys. Rev. D **16**, 1261 (1977).
[49] A. E. Brenner *et al.*, Phys. Rev. D **26**, 1497 (1982).
[50] H. Kichimi *et al.*, Phys. Rev. D **20**, 37 (1979).
[51] EHS-RCBC-Collaboration, J. L. Bailly *et al.*, Z. Phys. C **31**, 367 (1986).
[52] D. Antreasyan *et al.*, Phys. Rev. D **19**, 764 (1979).
[53] E735 Collaboration, T. Alexopoulos *et al.*, report 1992 (unpublished).
[54] E735 Collaboration, N. N. Biswas, in *Proceedings of the XXI International Symposium on Multiparticle Dynamics*, Wuhan, China, 1991, edited by L. Liu and Y. Wu (World Scientific, Singapore, 1992), p. 308.

[55] R. Castaldi and G. Sanguinetti, Annu. Rev. Nucl. Part. Sci. **35**, 351 (1985).
[56] M. N. Block and R. N. Cahn, Rev. Mod. Phys. **57**, 563 (1985).
[57] Particle Data Group, K. Hikasa *et al.*, Phys. Rev. D **45**, S1 (1992).
[58] D. S. Barton *et al.*, Phys. Rev. D **27**, 2580 (1983).
[59] NA34 Collaboration, T. Akesson *et al.*, Z. Phys. C **46**, 369 (1990).
[60] WA80 Collaboration, R. Albrecht *et al.*, Z. Phys. C **47**, 367 (1990).
[61] D. A. Garbutt *et al.*, Phys. Lett. **67B**, 355 (1977).
[62] H. Bialkowska, M. Gazdzicki, W. Retyk, and E. Skrzpczak, Z. Phys. C **55**, 491 (1992).
[63] P. Scubic *et al.*, Phys. Rev. D **18**, 3115 (1978).
[64] G. Battistoni, C. Forti, and J. Ranft, Astropart. Phys. (to be published).
[65] J. Durand and H. Pi, Phys. Rev. Lett. **58**, 2015 (1987).
[66] T. K. Gaisser and F. Halzen, Phys. Rev. Lett. **54**, 1754 (1987).
[67] R. S. Fletcher, T. K. Gaisser, P. Lipari, and T. Stanev, report, 1994 (unpublished).
[68] X. N. Wang and M. Gyulassy, Phys. Rev. D **44**, 3501 (1991).
[69] C. Forti, H. Biloken, B. d'Ettorre Piazzoli, T. K. Gaisser, L. Satta, and T. Stanev, Phys. Rev. D **42**, 3668 (1990).
[70] C. Forti (private communication).
[71] E. Gotsman, E. M. Levin, and U. Maor, Phys. Rev. D **49**, 4321 (1994).
[72] C. Albajar *et al.*, Nucl. Phys. **B335**, 261 (1990).
[73] EHS-RCBC-Collaboration, J. L. Bailly *et al.*, Z. Phys. C **35**, 295 (1987).
[74] H. H. Mielke, M. Föller, J. Engler, and J. Knapp, J. Phys. G **20**, 637 (1994).